NASA Technical Paper 1132

Effect of Design Changes on Aerodynamic and Acoustic Performance of Translating-Centerbody Sonic Inlets

Brent A. Miller

NASA

49

NASA Technical Paper 1132

Effect of Design Changes on Aerodynamic and Acoustic Performance of Translating-Centerbody Sonic Inlets

Brent A. Miller
Lewis Research Center
Cleveland, Ohio

NASA

National Aeronautics
and Space Administration

**Scientific and Technical
Information Office**

1978

EFFECT OF DESIGN CHANGES ON AERODYNAMIC AND ACOUSTIC PERFORMANCE
OF TRANSLATING-CENTERBODY SONIC INLETS

by Brent A. Miller

Lewis Research Center

SUMMARY

An experimental investigation was conducted to determine the effect of design changes on the aerodynamic and acoustic performance of translating-centerbody sonic inlets. Scale-model inlets with a diffuser exit diameter of 30.48 centimeters (12 in.) were tested in the Lewis Research Center's 2.74- by 4.58-meter (9- by 15-ft) V/STOL wind tunnel. The effects of centerbody position, entry lip contraction ratio, diffuser length, and diffuser area ratio on inlet total-pressure recovery, distortion, and noise suppression were investigated at static conditions and at a forward velocity of 41 meters per second (80 knots) over a range of incidence angles from 0° to 50°.

With the centerbody in the takeoff position (retracted), good aerodynamic and acoustic performance was attained at static conditions and at forward velocity for a wide range of incidence angles. At 0° incidence angle with a sound pressure level reduction of 20 decibels, the total-pressure recovery was 0.986. Pressure recovery at 50° was 0.981. With the centerbody in the approach position (extended), diffuser flow separation occurred at an incidence angle of approximately 20°. However, good performance was attained at lower angles.

With the centerbody in the takeoff position the ability of the inlet to tolerate high incidence angles was improved by increasing the lip contraction ratio. However, at static conditions with the centerbody extended in the approach position, an optimum lip contraction ratio appears to exist, with both thinner and thicker lips yielding reduced performance.

The effect of diffuser length on inlet performance was found to be a function of diffuser area ratio. For low area ratios the best performance was attained with the short diffuser; the long diffuser worked best at larger area ratios. As the desired approach weight flow was reduced relative to takeoff flow while maintaining inlet throat Mach number constant (resulting in a larger diffuser area ratio at approach), inlet aerodynamic performance was reduced for constant noise reduction.

A large improvement in inlet performance was found at forward velocity compared to static conditions. This suggests that static tests of sonic inlets may yield pessimistic results when compared with forward velocity performance.

INTRODUCTION

Aircraft engine noise radiated forward through the inlet can be suppressed by accelerating the inlet flow to sonic or near-sonic velocity in the inlet throat (refs. 1 to 8). This high inflow velocity does not allow the forward-propagating sound from the engine to escape from the inlet.

The noise reduction obtained with a high throat Mach number inlet, or sonic inlet, is a strong function of throat Mach number and does not become significant until the inlet average throat Mach number is higher than approximately 0.6. To reduce noise at both takeoff and approach airflows, variable inlet geometry is required in order to maintain the necessary inlet throat Mach number. The lower weight flow required at approach results in the greatest amount of diffusion. This condition, in general, becomes the controlling factor in the aerodynamic and mechanical design of variable-geometry sonic inlets.

Numerous types of variable-geometry sonic inlets have been tested (ref. 5). The translating-centerbody inlet has emerged as one of the more attractive concepts. The present investigation was conducted to determine experimentally the effect of changes in diffuser, entry lip, and centerbody design on the aerodynamic and acoustic performance of this type of sonic inlet. A baseline inlet design was selected with an approach weight flow equal to 80 percent of takeoff flow. The importance of the approach weight flow requirement was also investigated by changing the centerbody design to provide a constant inlet throat Mach number at approach weight flows equal to 86, 75, and 70 percent of takeoff flow. Tests were conducted with the centerbody in both the takeoff position (extended) and the approach position (retracted). In addition, the centerbody position was varied in increments between these two extremes for the baseline design.

The scale-model inlets used in this investigation, with a diffuser exit diameter (equivalent to the engine or fan diameter) of 30.48 centimeters (12 in.), were tested in the Lewis Research Center's 2.74- by 4.58-meter (9- by 15-ft) V/STOL wind tunnel. The tests were conducted by using a vacuum system and the appropriate valves and controls to induce inlet airflow. A siren was used to simulate engine machinery noise so that the noise suppression properties of the inlets could be determined. Tests were conducted at static conditions and at a tunnel airflow velocity of 41 meters per second (80 knots). Data were obtained at incidence angles of 0° to 50°. Measurements were made of the inlet total-pressure recovery, total-pressure distortion, and siren noise radiated from the inlet.

SYMBOLS

A   flow area

a   major axis of elliptical inlet lip

b   minor axis of elliptical inlet lip

D   diameter

$\mathcal{D}$ total-pressure distortion, [(Average total pressure) - (Minimum total pressure]/(Average total pressure)

e   axial length of centerbody forebody

f   thickness of entry lip external forebody

g   axial length of centerbody aftbody

L   length

M   Mach number

$\overline{M}$ average throat Mach number assuming one-dimensional flow

P   total pressure

$\overline{P}$ area-averaged total pressure

p   static pressure

$\Delta(SPL)$ reduction in siren-tone sound pressure level relative to that measured at an average throat Mach number of 0.60, dB

T   engine thrust

V_0 free-stream velocity (wind tunnel airflow), m/sec

W   inlet weight flow corrected to standard temperature and pressure

W^* inlet choking corrected weight flow assuming one-dimensional flow

w   axial length of entry lip external forebody

x   axial distance downstream of highlight or cowl throat

y   axial distance between cowl throat and position of centerbody maximum diameter

α incidence angle between inlet centerline and wind tunnel flow direction, deg

θ inlet diffuser wall angle, deg

Subscripts:

app   approach

BPF   siren blade passing frequency

c	cowl
cb	centerbody
ct	cowl throat
d	diffuser
e	diffuser exit
h	hub
hl	highlight
max	maximum
sep	flow separation
t	throat (minimum geometric flow area)
to	takeoff
0	wind tunnel airflow conditions
1	diffuser exit

APPARATUS AND PROCEDURE

Test Facility

Inlet tests were conducted in the Lewis Research Center's 2.74- by 4.58-meter (9- by 15-ft) V/STOL wind tunnel (ref. 9). A vacuum system was used in place of a fan or compressor to induce inlet flow. A schematic view of the test installation and facility is shown in figure 1.

A venturi, calibrated in place against a standard ASME bellmouth whose flow measurement had been corrected for boundary-layer growth, was used to measure inlet airflow. The scatter in the airflow calibration data was approximately ±0.2 percent at the design inlet mass flow of 11.68 kilograms per second (25.75 lbm/sec). Inlet airflow was remotely varied by using two flow control valves arranged to give both coarse and fine adjustment. Inlet incidence angle was also remotely varied by mounting the test apparatus on a turntable. A swivel joint, containing a low-leakage pressure seal, provided 360° rotation capability.

To determine the acoustic suppression properties of the inlet by using the vacuum flow system, a siren was installed in the duct downstream of the inlet. The siren was a 13.97-centimeter- (5.5-in.-) diameter single-stage fan modified by the addition of struts and a screen just upstream of the rotor to increase its noise level. The siren was lo-

cated approximately three inlet diameters downstream of the simulated fan face (fig. 1). Microphones were located in the wind tunnel approximately 20 meters (65 ft) upstream of the test section (also shown in fig. 1). The microphones were used to measure the siren noise transmitted through the inlet.

Inlet Design

A translating-centerbody sonic inlet is shown schematically in figure 2(a). The centerbody is shown in the three positions that would typically be required for takeoff, cruise, and approach, respectively. The inlet throat area obtained by varying the centerbody position is shown in figure 2(b) as a fraction of the takeoff throat area.

A critical factor in translating-centerbody sonic inlet design is the reduction in throat area at approach as compared with takeoff that is required to maintain a constant high throat Mach number for inlet noise suppression. This throat area change is directly related to the ratio of approach airflow to takeoff airflow, which is in turn determined by the ratio of approach thrust to takeoff thrust. The small increase in throat area that may be required between takeoff and cruise will also affect inlet design, but to a much lesser extent than the approach-to-takeoff variation. The relation between the approach-to-takeoff thrust ratio and the corresponding airflow ratio is shown in figure 3(a) for a turbofan engine with a takeoff fan pressure ratio of 1.5. Figure 3(b) shows the resulting diffuser area ratio required to maintain choked inlet flow. The assumption was made that the engine is designed for a fan face Mach number of 0.6 at takeoff airflow and that the fan efficiency remain constant at 0.85. The area ratio of figure 3(b) was then simply obtained from compressible flow calculations.

The circular symbols in figure 3(b) show the values of approach flow that were assumed in order to design the family of translating-centerbody inlets tested. A baseline design was selected that had an approach weight flow equal to 0.8 of the takeoff flow. As stated in reference 10, this is a representative value for jet-powered short takeoff and landing (STOL) aircraft. Inlets were also designed for flow ratios of 0.70 and 0.75, which are more representative of most existing conventional takeoff and landing (CTOL) aircraft. To evaluate what gains might be realized by increasing the approach airflow, inlets were also designed for a flow ratio of 0.86. The inlets tested had diffuser area ratios at approach ranging from 1.38 to 1.70 (fig. 3(b)).

The nomenclature used to describe the inlets tested is defined in figure 4. Inlets were fabricated in four major parts: the diffuser (two different designs), the removable entry lip (three designs), the nonrotating centerbody (seven designs), and cylindrical spacers used to position the centerbodies at different axial locations within the inlet.

Diffuser. - Table I describes the two diffuser designs. The major difference be-

tween the two diffusers was the overall length L_d, expressed in the table as a fraction of the exit diameter D_e. Both diffusers had a maximum local wall angle θ_{max} of 10.7^o.

The sketch on table I shows that the diffuser inflection point (location of θ_{max}) occurred well forward of the diffuser midpoint so that the maximum flow area change was attained with minimum centerbody travel. This design differs somewhat from the diffuser shape more generally encountered, where the inflection point is likely to occur further downstream toward the diffuser midpoint.

Entry lip. - The three entry lips tested are described in table II. The major geometric variable was internal lip contraction ratio $(D_{hl}/D_{ct})^2$. For each entry lip, an elliptical contour with a major-to-minor-axis ratio of 2 was used for the internal lip. This ratio is shown to be nearly optimum in reference 11. The external forebodies were designed by using the method of reference 12 to yield a cruise drag divergence Mach number of approximately 0.82 with cruise airflow equal to or greater than 0.95 of the takeoff airflow.

Centerbody. - The seven centerbodies tested are described in table III. Centerbodies A, B, C, and D were designed for the long diffuser. Centerbodies E, F, and G were designed for the short diffuser. The centerbodies differ only in the maximum diameter D_{cb} and the design of the aftbody downstream of the maximum diameter (fig. 4).

Centerbody maximum diameter is shown in table III as a fraction of hub diameter at the diffuser exit. Diameter ratios greater than 1 denote a bulbous-shaped centerbody. Centerbodies B and G, with a diameter ratio of 1.0, are cylindrical. Aftbody design is described in table III in terms of aftbody-length-to-centerbody-diameter ratio and maximum aftbody wall angle.

Models tested. - The diffusers, entry lips, and centerbodies described were combined to yield the inlet models tested. Figure 5 shows how the seven centerbodies and the appropriate spacers were used with the two diffusers to vary the inlet throat area. The baseline centerbody (design A) was tested with the long diffuser at five axial positions (fig. 5(a)), simulating centerbody movement from the takeoff position to the approach position. Approach throat area was varied about the baseline value by testing with centerbodies B, C, and D.

Centerbodies E and F, which differ only in aftbody design, were tested with the short diffuser at both takeoff and approach positions (fig. 5(b)). Centerbody G was tested only at approach. Centerbody positions between takeoff and approach were not investigated with the short diffuser.

All inlets tested are summarized in table IV. They are identified as models 1 to 18. Subsequent figures showing test results refer to these numerals for test model identifi-

cation. (Most of the tests, models 1 to 13, were conducted with the 1.38-contraction-ratio lip. Limited tests were conducted with the thinner lips.)

Instrumentation and Data Reduction

Aerodynamic data. - The location and extent of inlet steady-state pressure instrumentation are shown in figure 6. Two axial rows of 17 static-pressure taps each were located on the inlet, extending from the highlight to the rake measuring plane. One row was on the windward side of the inlet, and the other was on the leeward side. Section A-A shows the total-pressure rakes and static-pressure taps at the rake measuring plane. This is the approximate axial position that would normally lie in the plane of the fan face. Rake plane total-pressure measurements were made with both hub and tip boundary-layer rakes as well as total-pressure rakes spanning the entire annulus. Eight full-span total-pressure rakes were used with six equal-area-weighted tubes per rake. The hub and tip boundary-layer rakes each could take five total-pressure measurements.

Inlet total-pressure recovery $\overline{P}_1/P_0$ was computed from all the measured total pressures, including boundary-layer measurements, with the appropriate area-weighting terms. However, in computing inlet total-pressure distortion, boundary-layer measurements taken closer to the wall than the nearest tube on the six-element equal-area-weighted rakes were omitted. This resulted in excluding those measurements closer to the wall than 8.3 percent of the annulus area.

Acoustic data. - Noise data were taken with four microphones located in the wind tunnel settling chamber upstream of the test section (fig. 1). The hard walls of the wind tunnel approximate a reverberant chamber and eliminate any directional noise variation due to changing incidence angle. The microphone outputs were recorded on magnetic tape and then processed with a one-third-octave-band analyzer.

Figure 7 shows a one-third-octave-band analysis of typical noise spectra measured with a microphone. The upper curve shows the spectrum measured with both the siren and the wind tunnel in operation. Inlet average throat Mach number is 0.6, and there is little or no inlet noise suppression. The bottom curve shows wind-tunnel noise with the siren turned off. Data for both curves were taken at a free-stream velocity V_0 of 41 meters per second (80 knots). The spike in the siren spectrum at 5 kilohertz is at the siren rotor-blade passing frequency.

Noise data are presented in all subsequent figures for the one-third-octave band containing the 5-kilohertz spike. These data are shown in terms of the noise reduction parameter $\Delta(SPL)_{BPF}$, where $\Delta(SPL)_{BPF}$ is the reduction in siren-tone sound pressure level measured as the average throat Mach number was increased above 0.6. A correction of approximately 1.5 decibels was made in the siren source noise to account for

convective flow effects within the duct as inlet weight flow was increased to the maximum value. The sound pressure level at a throat Mach number of 0.6 was selected to be representative of the noise level for conventional inlets, where no appreciable fan or compressor noise reduction due to throat Mach number is observed. According to this definition, the maximum detectable noise reduction is approximately equal to the difference between the siren blade-passing-frequency spike at a throat Mach number of 0.6 and the tunnel background noise level. As shown in figure 7, this difference is approximately 30 decibels.

Test Procedure

The inlets were tested at static conditions and at a free-stream velocity of 41 meters per second (80 knots). Airflow was varied from that producing an average inlet throat Mach number of approximately 0.6 to the maximum value that could be passed by the inlet.

The data recorded to define the incidence angle at entry lip flow separation were obtained by setting the tunnel velocity and the inlet airflow. Data were then recorded in real time as the incidence angle was increased from zero at approximately 2 degrees per second. The data recorded at discrete angles were obtained by setting tunnel velocity and inlet weight flow while at a 0° incidence angle. Data were then recorded, and the incidence angle was increased to the next value. Data were again recorded and the procedure repeated.

RESULTS AND DISCUSSION

Inlet aeroacoustic performance, expressed as total-pressure recovery, steady-state total-pressure distortion, and sound pressure level reduction, is presented for each inlet tested. The results are discussed in four major sections in order to evaluate in a systematic manner the aeroacoustic performance of the large number of inlets tested. The four sections discuss the effect on inlet performance of centerbody position, entry lip contraction ratio, diffuser length, and diffuser area ratio at approach. With this method of data presentation the results obtained with any particular inlet configuration may appear in more than one section. In some instances, individual data points were subjected to detailed analysis in order to determine why inlet performance was affected by changes in geometry or operating conditions.

Centerbody Position

Data on the effect of centerbody position on inlet performance are presented at static conditions with the centerbody in the takeoff, intermediate, and approach positions. Comparison is made at a free-stream velocity of 41 meters per second (80 knots) between the takeoff and approach inlet geometries. Data presented in this section were obtained with the long diffuser and the 1.38-contraction-ratio lip.

Static operation. - The effect of centerbody position on inlet performance at static conditions was determined from tests of models 1 to 5 over a range of inlet weight flows (fig. 8). The measured inlet flow is shown as a fraction of the one-dimensional theoretical choking flow computed with the centerbody in the takeoff position. Theoretical choking flow limits computed for each centerbody position are shown by the crosshatched markings in the top part of the figure.

Several basic characteristics of sonic inlet performance can be seen by examining the data of figure 8. These data indicate a trend to lower pressure recovery and higher distortion as weight flow is increased toward the choking value. Note also the limited range of weight flow over which sound pressure level reduction is attained with a given centerbody position. This clearly shows the need for variable inlet geometry in order to attain significant sound pressure level reductions over a wide range of weight flows. For example, with the centerbody retracted in the takeoff position (test model 1, circular symbols), all sound pressure level reduction is lost for weight flow ratios below approximately 0.86. However, by extending the centerbody forward to a position near that of model 3, sound pressure level reductions in excess of 20 decibels are attainable at these reduced weight flows.

The relation between inlet aerodynamic performance, sound pressure level reduction, and inlet flow can most easily be seen by crossplotting the data of figure 8. This was done for three sound pressure level reductions and the results are shown in figure 9. Here, inlet total-pressure recovery and distortion are shown as fractions of the takeoff choking weight flow for sound pressure level reductions of 0, 10, and 20 decibels. With no sound pressure level reduction (0.6 throat Mach number) the total-pressure recovery was approximately 0.99 over the range of weight flow afforded by the variable throat area (fig. 9(a)). The total-pressure distortion ranged from 3 to 5 percent at the lower weight flows to a high of 9 percent at the highest flow. For sound pressure level reductions of 10 and 20 decibels a trend toward lower pressure recovery and higher distortion is evident with increased noise reduction. As might be expected, the poorest aerodynamic performance was attained with the centerbody fully extended in the approach position (test model 5), where the diffuser area ratio is the largest. A tendency can be noted for the best aerodynamic performance to occur with the centerbody in the intermediate position. For example, test model 3, with the centerbody midway between the

fully extended and fully retracted positions, yielded a total-pressure recovery of 0.981 with a sound pressure level reduction of 20 decibels. With the centerbody fully retracted in the takeoff position, the pressure recovery was 0.976.

The effectiveness of changing the inlet throat area by moving the inlet centerbody is shown in figure 10. Figure 10(a) illustrates the change in inlet weight flow that was measured as the centerbody was extended from the takeoff position (test model 1) to the approach position (test model 5) for a constant sound pressure level reduction of 20 decibels. Flow is shown as a fraction of the flow measured with the centerbody in the takeoff position (test model 1). The dashed line in figure 10(a) represents the flow variation expected based upon the change in inlet throat area with centerbody position for a constant throat Mach number (fig. 5(a)). According to the data, the approach flow is equal to 0.835 of the takeoff flow, as compared with an anticipated value of 0.8.

The reason for this discrepancy can be seen by examining the flow ratio shown in figure 10(b). This flow ratio denotes the fraction of the theoretical choking flow that could be passed by the inlet for each centerbody position. With the centerbody extended in the approach position the inlet was capable of passing approximately 0.99 of the theoretical choking weight flow. However, with the centerbody retracted in the takeoff position the inlet could pass only 0.955 of the theoretical limiting flow. This apparent reduction in flow capacity is attributed to the increased boundary-layer thickness resulting from the rearward movement of the throat and to the large axial and radial velocity gradients and flow curvature that exist within the skewed throat generated with the centerbody retracted. The reduction in the takeoff flow ratio is what accounts for the smaller-than-anticipated variation in flow between the takeoff and approach centerbody positions. This result suggests that, in order to maintain a noise suppression of 20 decibels and to obtain a 20-percent flow variation, it may be necessary to change the inlet throat area by somewhat more than 20 percent.

Performance at forward velocity and incidence angle. - Inlet models 1 and 5, representing the takeoff and approach configurations, respectively, were tested at a tunnel airflow velocity of 41 meters per second (80 knots) at incidence angles of 0° to 50°. With the inlet in the takeoff configuration, little difference in pressure recovery exists between operation at 0° and 50° incidence angles (top part of fig. 11(a)). However, incidence angle had a significant effect on distortion (middle part of fig. 11(a)). For example, at a flow ratio of 0.9 the distortion increased from approximately 0.02 to 0.10 in going from 0° to 50° incidence angle. The sound pressure level reduction was only slightly affected by increasing angle (bottom part of fig. 11(a)).

The change in inlet performance with forward velocity as compared with static operation is discussed in detail later (p. 16) for an inlet in the approach configuration. An examination of figures 8 and 11 shows some benefit with forward velocity for test model 1, where the centerbody is in the takeoff position.

With the centerbody extended in the approach position (fig. 11(b)) a large change in pressure recovery and distortion was noted as the incidence angle was increased from 0° to 30°, and finally to 40°. At an incidence angle of 30°, the pressure recovery measured at flow ratios above 0.75 was considerably below that measured at 0° (top part of fig. 11(b)). There was a corresponding increase in total-pressure distortion (middle part of fig. 11(b)). At 40° incidence angle the pressure recovery was lower and the distortion greater at all weight flows. To determine the reasons for this behavior, data points labeled 1, 2, and 3 in figure 11(b) are examined in more detail in figure 13. Meanwhile, the sound pressure level reduction attained with this inlet was only slightly affected by incidence angle (bottom of fig. 11(b)) even though large changes were noted in the aerodynamic performance.

The data of figure 11 were crossplotted in figure 12 to reveal the effect of incidence angle on total-pressure recovery and distortion for several sound pressure level reductions. With the centerbody retracted in the takeoff position, there was a progressive reduction in pressure recovery and an increase in distortion with increasing incidence angle and increasing sound pressure level reduction (fig. 12(a)). However, even at the rather severe 50° incidence angle, the inlet performed fairly well. At this condition a total-pressure recovery of 0.981 and a distortion of 0.125 were attained for a sound pressure level reduction of 20 decibels. At 0° incidence angle with 20 decibels of noise reduction, a pressure recovery of 0.986 and a distortion of 0.04 were recorded.

As would be expected from the data of figure 11(b), figure 12(b) shows that, with the centerbody extended, a large reduction in aerodynamic performance is suffered with increasing incidence angle. The reason for this behavior can be seen by considering the three data points labeled 1, 2, and 3 in the top part of figure 11(b). The axial distribution of static pressure on the inlet cowl surface for these three data points is plotted in figure 13(a), and the corresponding radial distribution of total pressure at the diffuser exit in figure 13(b).

The static-pressure distribution measured at 0° incidence angle (data point 1) shows a minimum static pressure (maximum surface Mach number) occurring near the cowl throat plane with a smooth continuous diffusion to the diffuser exit. As might be expected, the corresponding radial total-pressure profiles (fig. 13(b)) reveal a symmetric distribution of total-pressure loss at the diffuser exit at 0° incidence angle. No flow separation is evident. This is reflected in the high total-pressure recovery, approximately 0.992, measured at this point.

With an increase in the incidence angle to 30° (data point 2), the cowl static-pressure distribution exhibits a downturn and an flat spot, usually indicative of separation and loss of diffusion, at a location just downstream of the $x/L_c = 0.33$ position. This apparent separation has occurred at approximately the axial location of maximum diffuser wall angle. However, further downstream in the diffuser, between x/L_c of 0.64

and 0.72, it appears as though the flow may have partially reattached. The corresponding radial total-pressure profile at the diffuser exit clearly shows the total-pressure loss experienced on the windward side due to this diffuser flow separation. The shape of the profile suggests that some degree of reattachment has occurred. This local diffuser separation, with possibly some degree of reattachment, yielded a total-pressure recovery of 0.986, down from the recovery of 0.992 recorded at the same weight flow and 0° incidence angle.

At 40° incidence angle (data point 3), the cowl static-pressure distribution of figure 13(a) reveals that the location of flow separation has moved forward toward the throat. No clear indication of flow reattachment can be detected downstream in the diffuser, although some diffusion is suggested by the gradual reduction in static pressure toward the diffuser exit. The surface static pressures upstream of the separated region have increased over those at 30° incidence angle because of a drop in inlet weight flow resulting from flow separation. Examination of the radial total-pressure contours suggests separated flow persisting to the diffuser exit on the windward side. However, the total-pressure profile indicates fully attached flow with little loss on the leeward side. This attached flow may result in some net diffusion and could account for the apparent diffusion detected toward the diffuser exit. This diffuser separation occurring on the windward side, and apparently persisting to the location of the total-pressure rakes, reduced total-pressure recovery to 0.977. (At incidence angles from 0° to 30° (fig. 11(b)), the total-pressure recovery was approximately 0.993.) Figure 13(b) also shows no total-pressure losses occurring as a result of flow separation from the centerbody for any of the three data points examined.

As just discussed, the tendency to poor aerodynamic performance at elevated incidence angles with the centerbody extended in the approach position has been traced to flow separation in the diffuser on the windward side. Traces of inlet surface static pressure and diffuser exit total pressure plotted as a continuous function of incidence angle (not shown in this report) reveal that the separation occurred at an incidence angle of approximately 20°. The inlet performed well below this angle.

These tests were conducted with relatively small (30.48-cm (12-in.) diffuser exit diameter), smooth surface models; and it is possible that this susceptibility to flow separation could be reduced somewhat by introducing surface roughness to hasten the laminar-to-turbulent boundary-layer transition. Vortex generators, or possibly some other method of flow control, might also show an advantage. The results presented in reference 6 from tests of a similar inlet suggest that tolerance to incidence angle might be improved by simply retracting the centerbody a small amount. However, this does have the disadvantage of reducing the throat area change between the approach and takeoff centerbody positions.

Lip Contraction Ratio

The effect on aeroacoustic performance of lip contraction ratio at takeoff with the long diffuser was investigated with test models 1, 14, and 16 at contraction ratios of 1.38, 1.34, and 1.30 (table IV), respectively. The effect of these same contraction ratios at approach was determined with models 5, 15, and 17. The approach condition was investigated with the short diffuser by testing models 13 and 18 at contraction ratios of 1.38 and 1.30, respectively.

Takeoff. - The effect of decreasing the inlet lip contraction ratio from 1.38 to 1.34, and finally to 1.30, at takeoff was investigated. Total-pressure recovery and distortion as a function of sound pressure level reduction are shown in figure 14 for each of the three inlet lips at each of three test conditions. Figure 14(a) shows the performance at static conditions, 14(b) at 0° incidence angle and 41-meter-per-second (80-knot) free-stream velocity, and 14(c) at 40° incidence angle for the same free-stream velocity. These test conditions were judged sufficient to yield results indicative of what might be expected with each inlet during ground and takeoff operations.

Changes in lip contraction ratio had little effect on inlet performance at takeoff for the three test conditions just noted. However, model 14, with the 1.34-contraction-ratio lip, does show some tendency to yield the highest recovery and lowest distortion of the three designs, especially at 40° incidence angle.

While contraction ratio does not appear to be significant at the three test conditions of figure 14, it is of importance when operating at high incidence angles. Figure 15 shows the incidence angle required to produce flow separation from the inlet lip for each of the three designs. The angle is shown as a function of flow ratio and average throat Mach number. For flow ratios above approximately 0.85, where noise suppression becomes significant (fig. 11(a)), the inlet with the largest contraction ratio is clearly superior in terms of flow separation angle. However, separation-free operation at incidence angles greater than 45° was attained with even the thinnest lip.

The method of data presentation shown in figure 14 is useful in that it allows the acoustic and aerodynamic trade-offs to be directly compared for different inlet designs. For this reason, this same method of data presentation is used extensively throughout the remaining sections of this report.

Approach. - The effect of contraction ratio on inlet performance with the centerbody in the approach position is shown in figure 16. Test models 5, 15, and 17 differed from the models discussed in the previous two figures only in centerbody position. Inlet performance was strongly affected by lip contraction ratio at static conditions (fig. 16(a)). As before, contraction ratio did not appear to be a significant factor at 0° incidence angle and 41-meter-per-second (80-knot) free-stream velocity (fig. 16(b)). The reduced performance at angle of attack with the centerbody extended (fig. 16(c)), discussed in

figures 11 and 12 for test model 5, is again clearly evident. For example, figure 16(b) shows that a total-pressure recovery of approximately 0.99 can be attained with a sound pressure level reduction of 20 decibels at 0° incidence angle. However, with an increase in the incidence angle to 30°, the total-pressure recovery drops to approximately 0.965 for the same noise reduction. Figure 16(c) suggests that this change in performance with angle of attack at approach was only slightly affected by lip thickness, at least for the range of thicknesses tested.

Static performance was markedly poorer with the thick-lip inlet (test model 5) than with the two thinner-lip models. The inlet with the intermediate lip thickness (test model 15) showed the best performance. This suggests that an optimum lip contraction ratio may exist. This result was unexpected, and data points labeled 1 and 2 were examined in some detail in an attempt to determine the cause of this behavior.

Axial static-pressure and radial total-pressure distributions were measured for data points 1 and 2 (fig. 17). The pressure distribution of figure 17(a) suggests that, with the 1.38-contraction-ratio lip, partial diffuser flow separation occurred just upstream of the location of maximum diffuser wall angle. This separation resulted in the total-pressure loss noted in figure 17(b). The tendency to diffuser flow separation observed with the thick-lip inlet may result from an increase in boundary-layer thickness at the cowl throat plane because of the greater lip surface area. For example, the surface distance between the highlight and the cowl throat plane was increased 25 percent by raising the contraction ratio from 1.3 to 1.38. The resulting thick boundary layer would be less able to withstand the strong adverse pressure gradient downstream of the cowl throat. This effect may dominate diffuser performance even though the highest local surface velocities were attained with the thin lip (fig. 17(a)).

The effect of contraction ratio on performance with the short diffuser at approach is shown in figure 18. Again, at static conditions, the thin-lip inlet gave the best performance. Lip contraction ratio did not affect performance at forward velocity and 0° incidence angle (fig. 18(b)). However, at 30° incidence angle (fig. 18(c)), the best performance was attained with the thin lip. Recall that, with the long diffuser, no effect of lip contraction ratio was noted at this condition (fig. 16(c)). This suggests that the design of the inlet lip for best inlet operation is closely related to diffuser design.

Diffuser Length

Two diffusers were tested to determine the effect of diffuser length on inlet aeroacoustic performance. The long diffuser had a length-to-exit-diameter ratio L_d/D_e of 0.875. The length-to-exit-diameter ratio of the short diffuser was 0.667. These diffusers were tested in both the takeoff and approach configurations with the 1.38-

contraction-ratio lip.

Takeoff. - Inlet performance measured with the centerbody in the takeoff position is shown in figure 19. The highest total-pressure recoveries and lowest distortions were measured with the short diffuser (models 10 and 9). Lower total-pressure recovery was measured with the long diffuser because, as explained in reference 8, it has more wetted surface area than the short diffuser. Comparison of models 9 and 10 shows no effect due to changing centerbody design (centerbodies E and F).

Approach. - Inlet performance with the centerbody in the approach position was determined for two diffuser area ratios A_e/A_t. The data in figure 20 were obtained with cylindrical centerbodies at a diffuser area ratio of 1.38. Unlike figure 19 for the takeoff configuration, this figure does not show any significant change in performance with diffuser length. A possible explanation for this may lie in a trade-off between the total-pressure loss generated as a result of an increased rate of diffusion and that resulting from more wetted surface area. In the data of figure 20, the additional total-pressure loss generated by increasing the diffuser length may have been compensated for by a reduction in the diffusion loss resulting from the lower diffusion rate obtained with the long diffuser. This compensating effect of diffusion rate may be small at takeoff, where the diffuser area ratio was only 1.19.

This explanation for the measured change in performance with increased diffuser length is consistent with the data of figure 21. These data were obtained at approach with the diffuser area ratio increased to 1.49. They show that the long diffuser gave the best performance. With this contraction ratio the losses due to diffusion were larger with the short diffuser. Increasing diffuser length, therefore, improved inlet performance through a reduction in diffusion rate even though the wetted area was increased. These results show that an optimum diffuser length exists for each diffuser area ratio. This is in agreement with the design techniques for simple conical diffusers (ref. 13).

The reduced performance noted in figures 20 and 21 at 30° incidence angle resulted from diffuser flow separation. This diffuser flow separation and the resulting total-pressure loss at the diffuser exit are shown in figure 22. These static- and total-pressure distributions were obtained for data points labeled 1 and 2 for test model 13 (fig. 21). Comparison of the inlet cowl axial static-pressure distributions measured at 0° and 30° incidence angles (fig. 22(a)) clearly reveals diffuser flow separation occurring at an x/L_c of approximately 0.3. This type of separation was discussed in detail with test model 5 (fig. 13).

Diffuser Area Ratio at Approach

Diffuser area ratios at approach of 1.38, 1.49, 1.58, and 1.70 were tested with the long diffuser and the 1.38-contraction-ratio lip. As shown by the sketch in figure 23, the diffuser area ratio was changed by varying the centerbody design. Inlet aerodynamic and acoustic performance is plotted in figure 23 as a function of the takeoff choking weight flow. Computed flow limits shown on this figure by the crosshatching marks indicate the reduction in approach flow resulting from increasing the centerbody diameter. The data of this figure were crossplotted in figure 24 to illustrate how diffuser area ratio affected the trade-off between aerodynamic and acoustic performance.

As diffuser area ratio was increased, pressure recovery was reduced and distortion was increased for a constant sound pressure level reduction. One exception to this trend can be seen in figure 24(b), where the best aerodynamic performance was not attained with the inlet having the lowest diffuser area ratio. Here, the baseline inlet (test model 5) performed slightly better than the inlet with the lowest area ratio. Data points labeled 1 to 6 in figure 24 are analyzed in detail in the next section.

Pressure distributions. - The effect of diffuser area ratio on inlet performance can be seen by examining the pressure distributions shown in figure 25. Pressure distributions were measured at static conditions with models 6 and 8 at the smallest and largest diffuser area ratios (fig. 25(a)). The pressure distributions shown are for data points labeled 1 and 2 in figure 24. The inlet cowl axial static-pressure distribution for test model 8, shown in figure 25(a) by the triangular symbols, suggests that some diffuser separation may have occurred in the region of maximum diffuser wall angle. This possible separation, or perhaps a rapid increase in boundary-layer thickness due to diffusion, resulted in the reduced total pressure measured at the diffuser exit (shown at the right of the figure). At 30° incidence angle (fig. 25(b)), diffuser flow separation has apparently occurred with the large-area-ratio diffuser (test model 8). This is reflected in both the surface static-pressure and radial total-pressure distributions. However, at this incidence angle, the flow is still apparently attached with test model 6. The data do not indicate any flow separation occurring on the centerbody.

In summary, figure 25 shows that the reduced aerodynamic performance with large-area-ratio diffusers results from total-pressure losses caused by increased diffusion and flow separation.

Effect of forward velocity. - The effect of forward velocity on inlet performance is shown in figure 26 as a function of sound pressure level reduction and flow ratio W_{app}/W_{to}^*. Comparison of the solid and dashed lines for a given sound pressure level reduction reveals a large improvement in aerodynamic performance at a 41-meter-per-second (80-knot) free-stream velocity as compared with static conditions. For example, with test model 8 for a sound pressure level reduction of 20 decibels, the pressure re-

covery increased from 0.944 to 0.970 as a result of free-stream velocity. This suggests that static tests will yield pessimistic results when compared with forward-velocity performance.

The improvement in performance with forward velocity can be seen in more detail in figure 27, where static- and total-pressure distributions are shown for the data points labeled 5 and 6 in figure 24 (test model 7). Although figure 27(a) does not indicate diffuser flow separation at static conditions, figure 27(b) does show a loss in total pressure toward the tip. This may result from the higher surface velocities near the highlight at static conditions. This loss in total pressure was largely eliminated with forward velocity, resulting in improved inlet performance. There was no indication of total-pressure losses occurring near the hub.

SUMMARY OF RESULTS

An experimental investigation was conducted to determine the effect of design changes on the aerodynamic and acoustic performance of translating-centerbody sonic inlets. Scale-model inlets with a diffuser exit diameter of 30.48 centimeters (12 in.) were tested in the Lewis Research Center's 2.74- by 4.58-meter (9- by 15-ft) V/STOL wind tunnel. The principal results of this investigation are as follows:

1. With the centerbody retracted in the takeoff position, aerodynamic and acoustic performance was good at static conditions and at a forward velocity of 41 meters per second (80 knots) for a wide range of incidence angles. For example, at 50° incidence angle with a sound pressure level reduction of 20 decibels, the total-pressure recovery was 0.981, with a total-pressure distortion of 0.125. At 0° incidence angle with 20 decibels noise reduction, the pressure recovery was 0.986, with a total-pressure distortion of 0.04.

2. Aerodynamic and acoustic performance was good with the centerbody extended in the approach position for incidence angles below approximately 20°. At higher incidence angles, flow separation occurred within the diffuser, resulting in increased total-pressure distortion and reduced total-pressure recovery. The flow did not separate from the centerbody.

3. The effect of inlet lip contraction ratio on the inlet performance was most pronounced at high incidence angles with the centerbody retracted (takeoff) and at static conditions with the centerbody extended (approach). At all other conditions, inlet performance was only slightly altered by changing the contraction ratio from 1.30 to 1.34, and finally to 1.38. With the centerbody retracted the ability of the inlet to tolerate high incidence angles was improved by increasing the lip contraction ratio. However, at static conditions with the centerbody extended, an optimum contraction ratio appears

to exist, with both thick and thin lips yielding reduced performance.

4. The effect of diffuser length on inlet performance is a function of diffuser area ratio. At takeoff with the centerbody retracted, yielding a diffuser area ratio of 1.19, the best aerodynamic and acoustic performance was attained with the short diffuser. No significant effect of diffuser length was detected when the diffuser area ratio was increased to 1.38. However, with a further increase in area ratio to 1.49, the best performance was attained with the long diffuser. These results show that an optimum inlet length exists for each diffuser area ratio.

5. As approach weight flow was reduced relative to takeoff flow (resulting in an increase in diffuser area ratio for a constant throat Mach number), pressure recovery was reduced and distortion was increased for a constant sound pressure level reduction. The reduced aerodynamic performance resulted from increased diffusion losses and in some cases diffuser flow separation. There was no indication of flow separation on the centerbody.

6. Inlet performance improved at forward velocity as compared with static conditions. This improvement was particularly large for those inlets having the largest diffuser area ratio. For example, with a diffuser area ratio of 1.7 and a sound pressure level reduction of 20 decibels, the pressure recovery increased from 0.944 and 0.970 in going from static conditions to a forward velocity of 41 meters per second (80 knots). Thus, static tests of large-area-ratio sonic inlets may yield pessimistic results as compared with forward-velocity performance.

Lewis Research Center,
National Aeronautics and Space Administration,
Cleveland, Ohio, September 20, 1977,
505-03.

REFERENCES

1. Miller, Brent A.; and Abbott, John M.: Aerodynamic and Acoustic Performance of Two Choked-Flow Inlets under Static Conditions. NASA TM X-2629, 1972.

2. Miller, Brent A.; and Abbott, John M.: Low-Speed Wind Tunnel Investigation of the Aerodynamic and Acoustic Performance of a Translating-Centerbody Choked-Flow Inlet. NASA TM X-2773, 1973.

3. Klujber, F.: Results of an Experimental Program for the Development of Sonic Inlets for Turbofan Engines. AIAA Paper 73-222, Jan. 1973.

4. Groth, H. W.: Sonic Inlet Noise Attenuation and Performance with a J-85 Turbojet Engine as a Noise Source. AIAA Paper 74-91, Jan. 1974.

5. Abbott, J. M.: Aeroacoustic Performance of Scale Model Sonic Inlets - Takeoff/Air Approach Noise Reduction. AIAA Paper 75-202, Jan. 1975.

6. Hickcox, T. E.; et al.: Low Speed and Angle of Attach Effects on Sonic and Near-Sonic Inlets. (D6-42392, Boeing Commercial Airplane Co.; NASA Contract NAS3-18035.) NASA CR-134778, 1975.

7. Miller, B. A.; Dastoli, B. J.; and Wesoky, H. L.: Effect of Entry-Lip Design on Aerodynamics and Acoustics of High Throat Mach Number Inlets for the Quiet, Clean, Short-Haul Experimental Engine. NASA TM X-3222, 1975.

8. Miller, B. A.: Experimentally Determined Aeroacoustic Performance and Control of Several Sonic Inlets. AIAA Paper 75-1184, Sept. 1975.

9. Yuska, Joseph A.; Diedrich, James H.; and Clough, Nestor: Lewis 9- by 15-Foot V/STOL Wind Tunnel. NASA TM X-2305, 1971.

10. Hodge, C. G.; Winslow, L. J.; and Wood, S. K.: The Effect of Inlet-Noise Suppression on Propulsion System Design. AIAA Paper 73-1294, Nov. 1973.

11. Albers, James A.; and Miller, Brent A.: Effect of Subsonic Inlet Lip Geometry on Predicted Surface and Flow Mach Number Distributions. NASA TN D-7446, 1973.

12. Hancock, J. P.; and Hinson, B. L.: Inlet Development for the L-500. AIAA Paper 69-448, June 1969.

13. Henry, John R.; Wood, Charles C.; and Wilbur, Stafford W.: Summary of Subsonic-Diffuser Data. NACA RM L56F05, 1956.

TABLE I. - DIFFUSER DESIGN

[Exit diameter, D_e, 30.48 cm.]
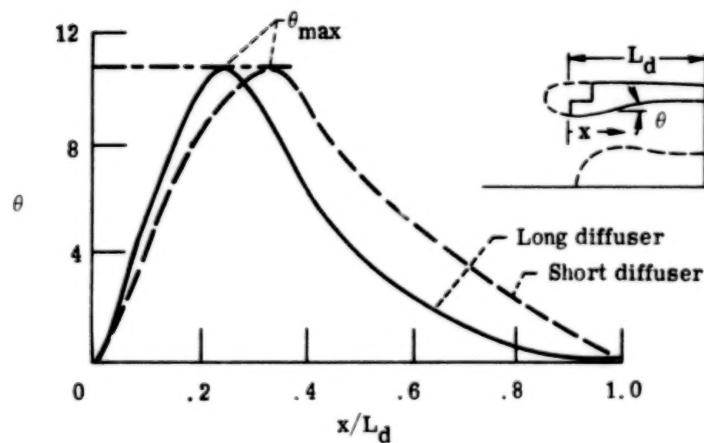
Geometric variable	Long diffuser	Short diffuser
Ratio of diffuser length to exit diameter, L_d/D_e	0.875	0.667
Average wall angle, $\tan^{-1}\left(\dfrac{D_e - D_{ct}}{2L_d}\right)$, deg	4.0	5.3
Maximum wall angle, θ_{max}, deg	10.7	10.7
Diffuser exit diameter ratio, D_h/D_e	0.4	0.4

TABLE II. - ENTRY LIP DESIGN

[Internal lip contour, ellipse; internal lip proportions, a/b, 2.0; ratio of external forebody length to maximum diameter, w/D_{max}, 0.375; external forebody contour, NACA-1.]

Geometric variable	Entry lip		
	1	2	3
Internal lip contraction ratio, $(D_{hl}/D_{ct})^2$	1.38	1.34	1.30
External forebody diameter ratio, D_{hl}/D_{max}	0.86	0.845	0.833
External forebody proportions, w/f	5.30	4.86	4.50

TABLE III. - CENTERBODY DESIGN

[Location of maximum afterbody wall angle, 50 percent g; afterbody surface contour, cubic; ratio of forebody length to maximum diameter, e/D_{cb}; forebody contour, ellipse.]

Geometric variable	Long diffuser				Short diffuser		
	Centerbody design						
	A	B	C	D	E	F	G
Ratio of maximum diameter to hub diameter, D_{cb}/D_h	1.125	1.0	1.220	1.310	1.125	1.125	1.0
Ratio of aftbody length to maximum diameter, g/D_{cb}	0.742	0.742	0.854	0.960	0.648	0.463	0.520
Maximum aftbody wall angle, $\theta_{cb,max}$, deg	6.0	0	9.0	10.4	7.3	10.2	0

TABLE IV. - TRANSLATING-CENTERBODY SONIC INLET TEST MATRIX

Entry lip contraction ratio, $(D_{hl}/D_{ct})^2$	Ratio of diffuser length to exit diameter, L_d/D_e												
	0.875								0.667				
	Centerbody position												
	Takeoff	Intermediate			Approach				Takeoff		Approach		
	Centerbody design												
	A				B	C	D		E	F	G	E	F
	Throat area ratio, $A_t/A_{t,to}$												
	1.00	0.92	0.86	0.82	0.80	0.86	0.75	0.70	1.00		0.86	0.80	
	Diffuser area ratio, A_e/A_t												
	1.19	1.29	1.38	1.45	1.49	1.38	1.58	1.70	1.19		1.38	1.49	
	Model tested												
1.38	1	2	3	4	5	6	7	8	9	10	11	12	13
1.34	14	---	---	---	15	---	---	---	---	---	---	---	---
1.30	16	---	---	---	17	---	---	---	---	---	---	---	18
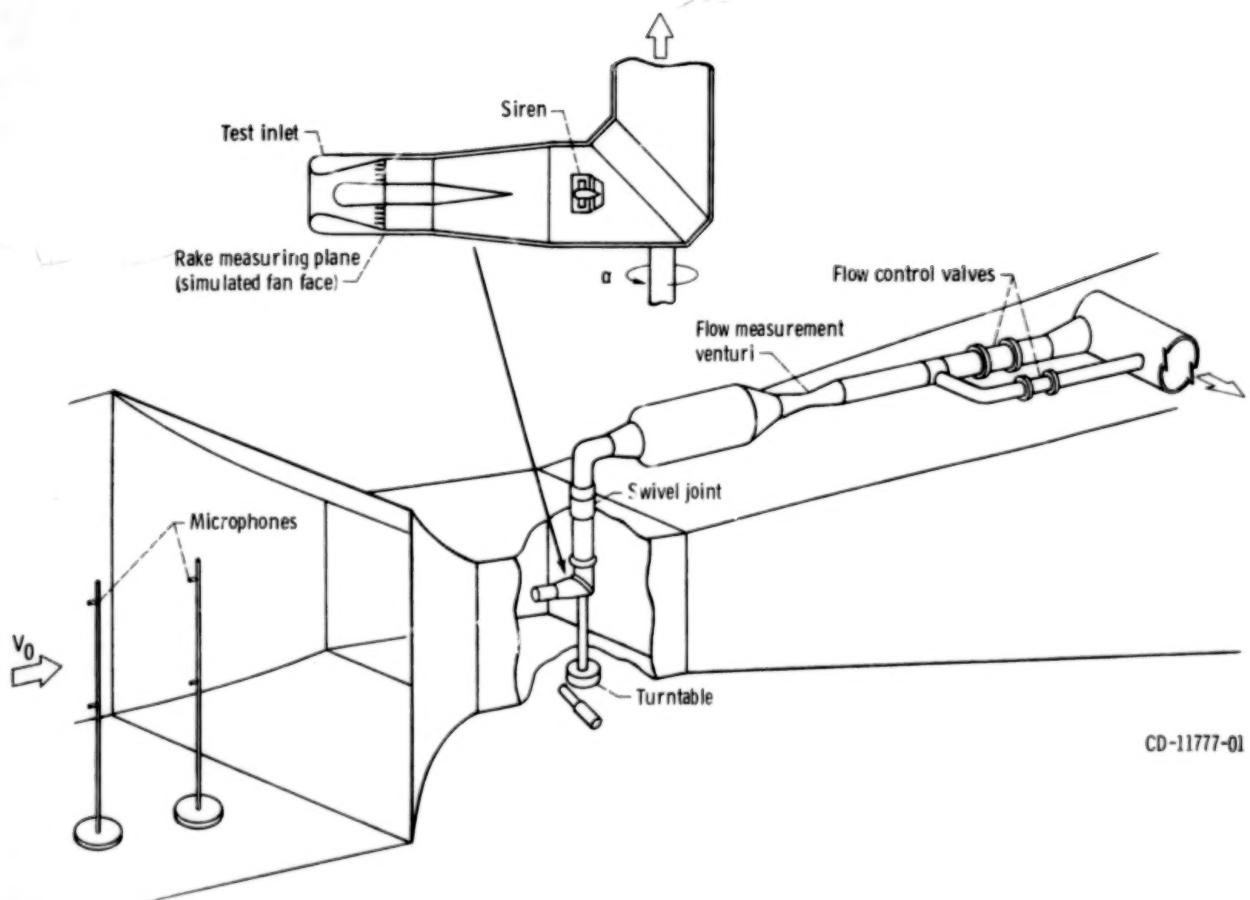
Figure 1. - V/STOL wind tunnel, showing model arrangement and microphone locations.

CD-11777-01

23.

(a) Inlet schematic (three centerbody positions).

(b) Inlet throat area for continuously variable centerbody position.
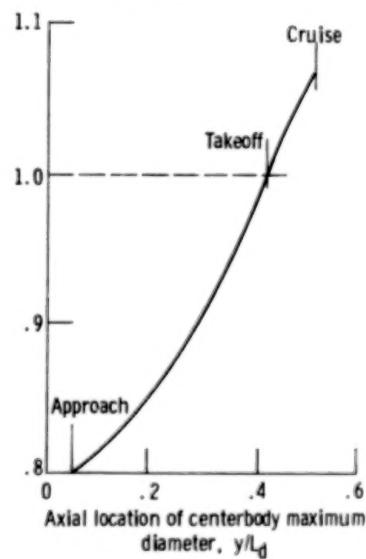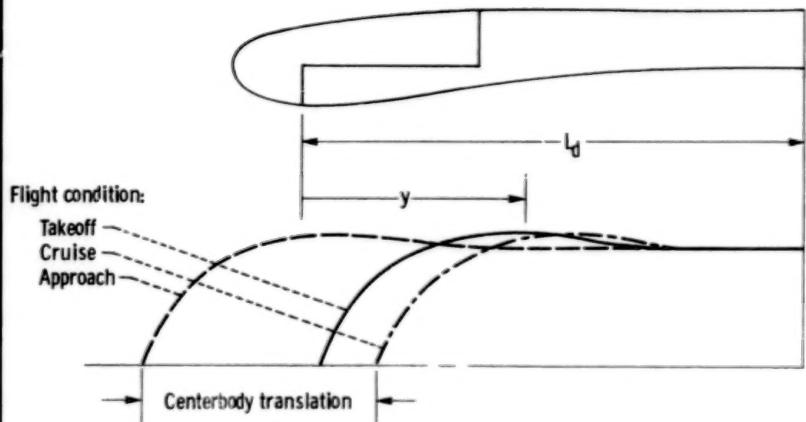
Figure 2. - Translating-centerbody sonic inlet.

(a) Static thrust at reduced weight flow and fan takeoff pressure ratio of 1.5.

(b) Diffuser area ratio at approach thrust with choked inlet throat.
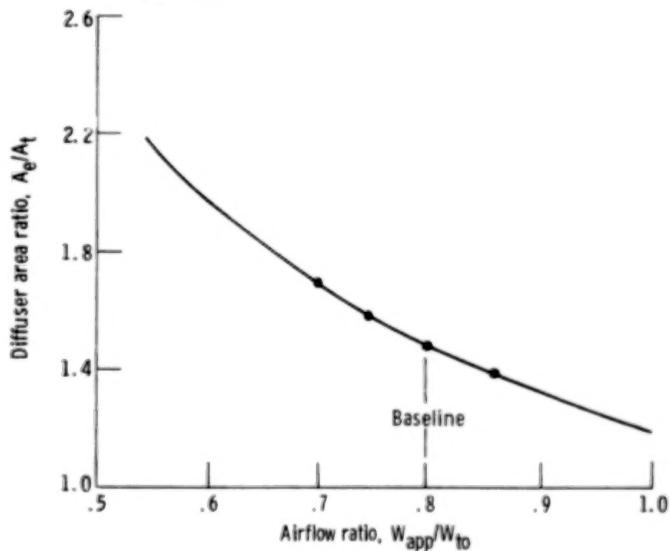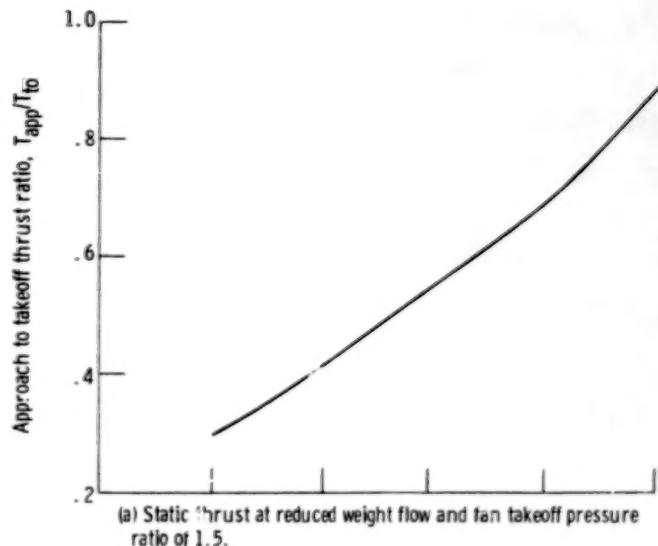
Figure 3. - Effect of approach thrust requirement on sonic inlet weight flow and diffuser area ratio. Diffuser exit Mach number at takeoff airflow, M_e, 0.60.
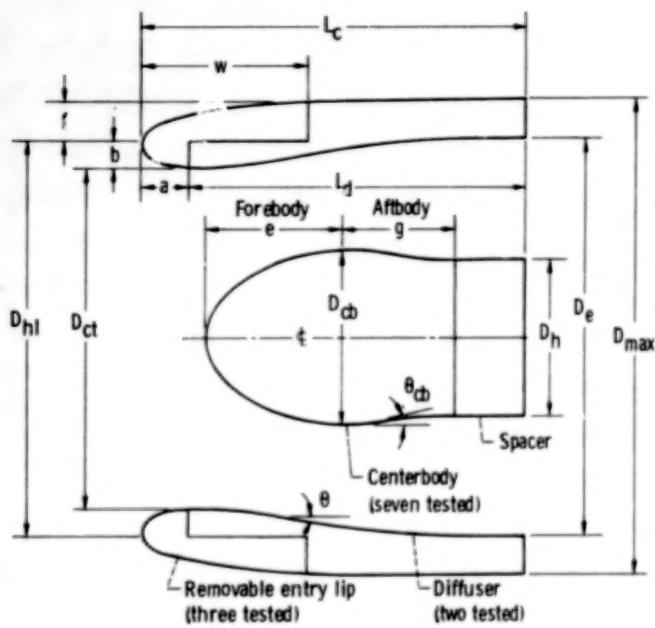
Figure 4. – Inlet nomenclature.

(a) Long diffuser; diffuser length to exit diameter ratio, L_d/D_e, 0.875.
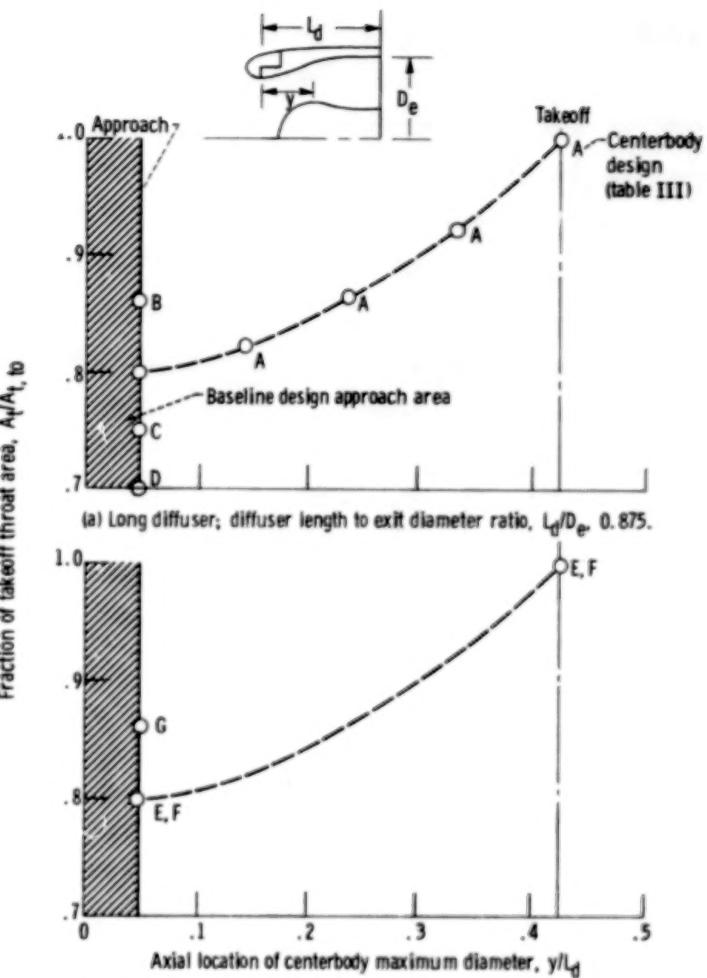
(b) Short diffuser; diffuser length to exit diameter ratio, L_d/D_e, 0.667.

Figure 5. – Effect of centerbody position and centerbody design on inlet throat area. Diffuser area ratio at takeoff, $A_e/A_{t, to}$, 1.19.

25.
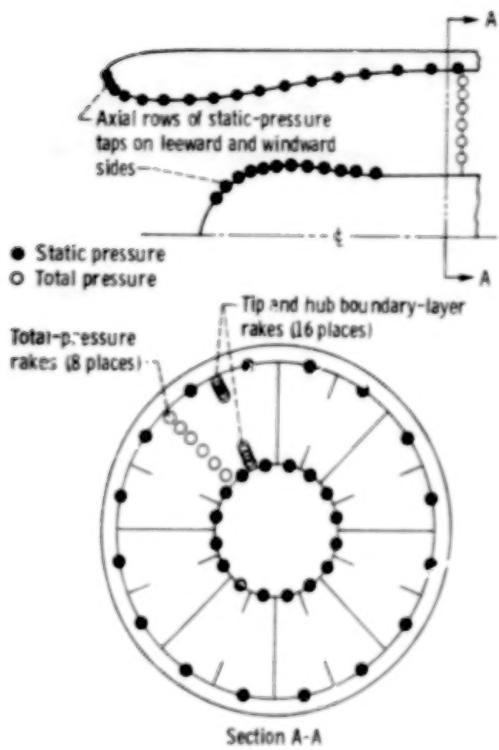
Figure 6. - Pressure instrumentation.
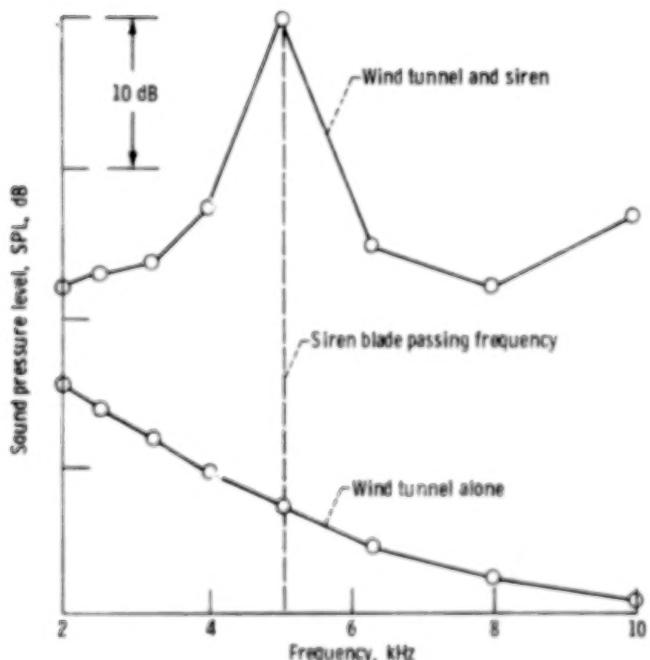
Figure 7. - One-third-octave band spectra showing characteristics of siren and wind tunnel noise. Inlet average throat Mach number, M_t, 0.6; free-stream velocity, V_0, 41 m/sec (80 knots).

26.
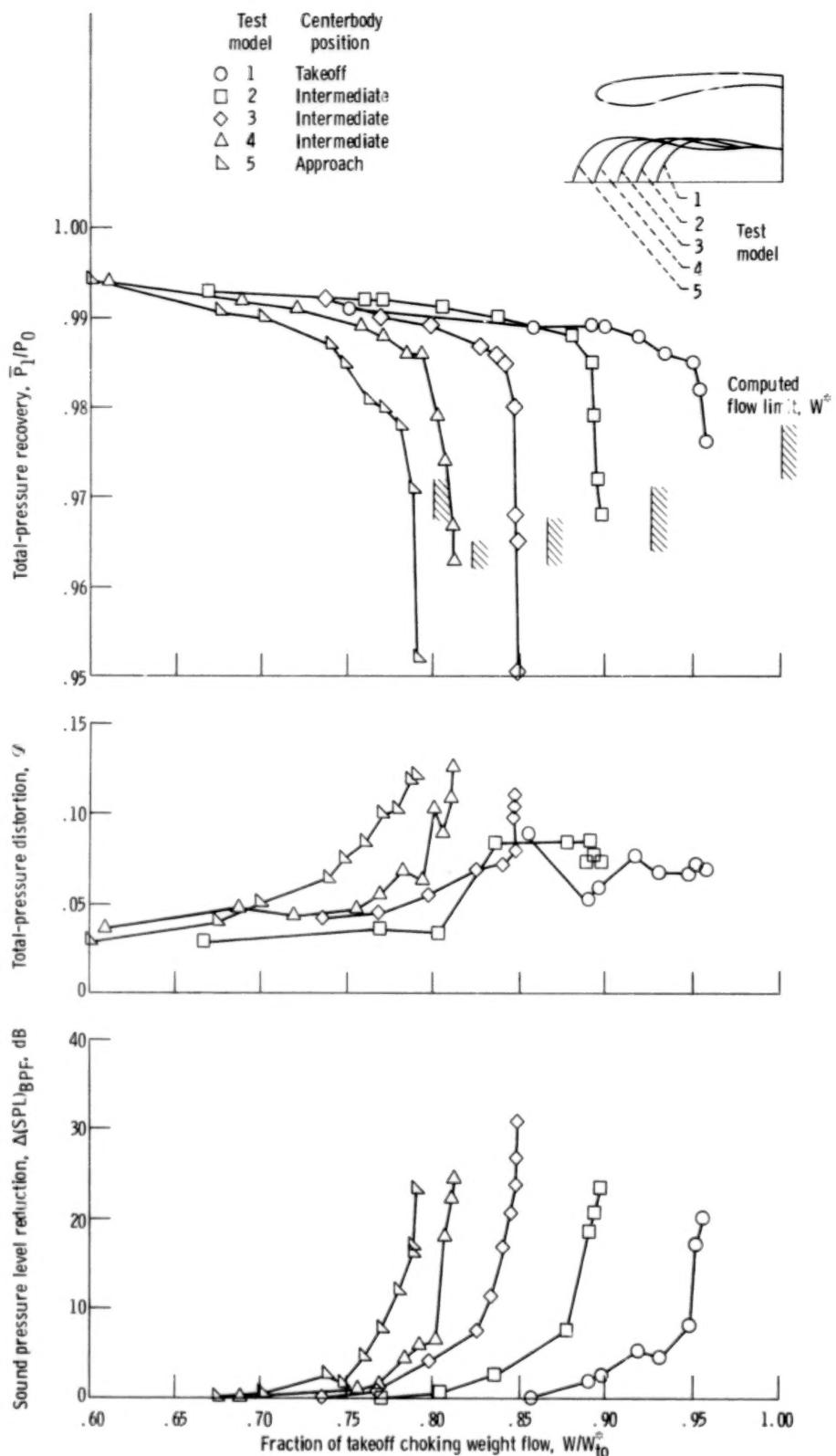
Figure 8. – Effect of centerbody position on aeroacoustic performance at static conditions. Long diffuser; centerbody A; inlet lip contraction ratio, 1.38.

27.
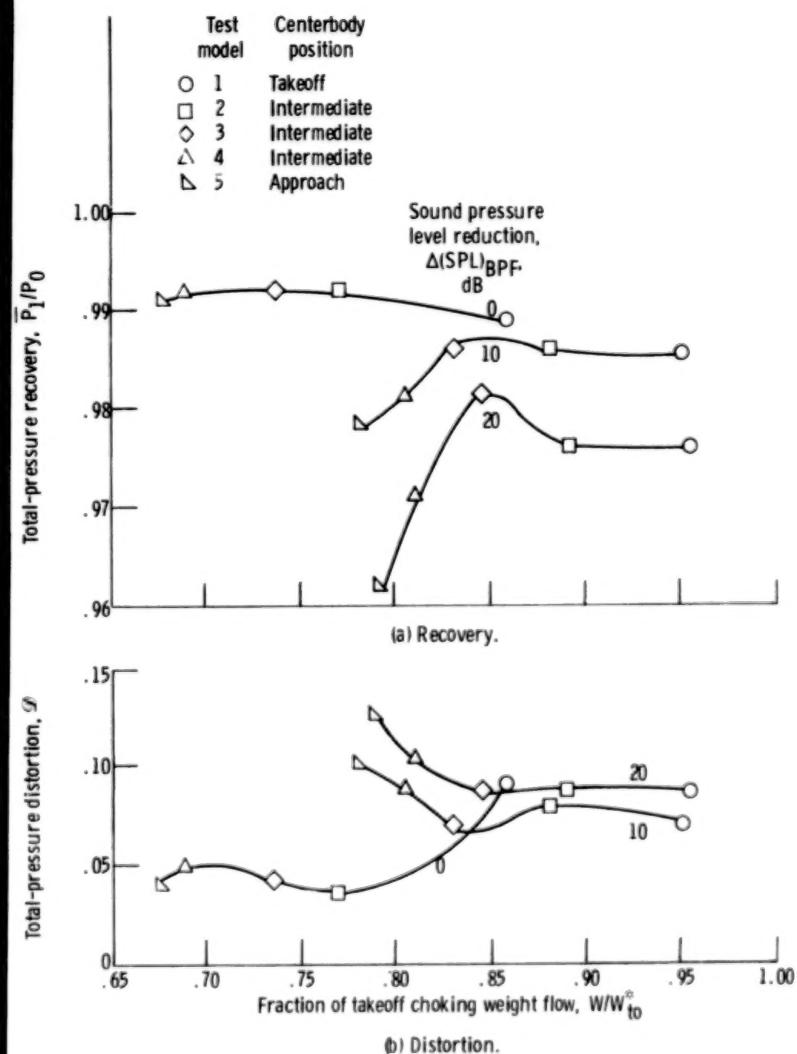
Figure 9. - Effect of sound pressure level reduction and centerbody position on inlet aerodynamic performance at static conditions. (Data are a crossplot of fig. 8.)

(a) Recovery.

(b) Distortion.

(a) Fraction of takeoff weight flow at constant SPL reduction of 20 dB.

(b) Fraction of theoretical choking weight flow at maximum inlet flow.
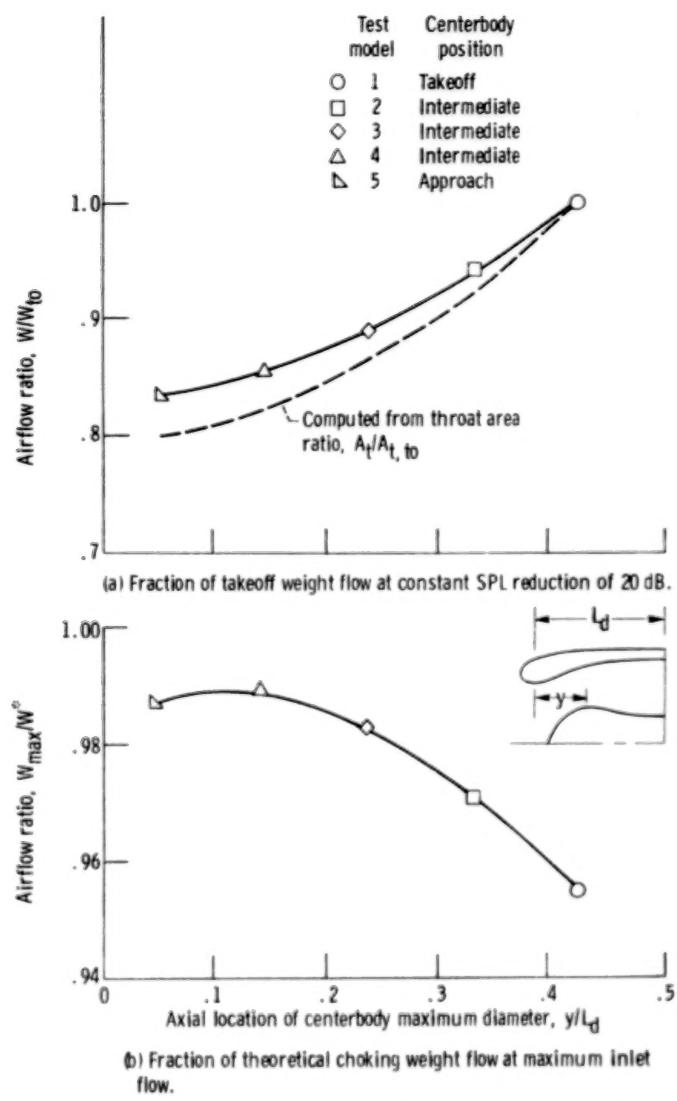
Figure 10. - Effect of centerbody position on measured inlet weight flow at static conditions.
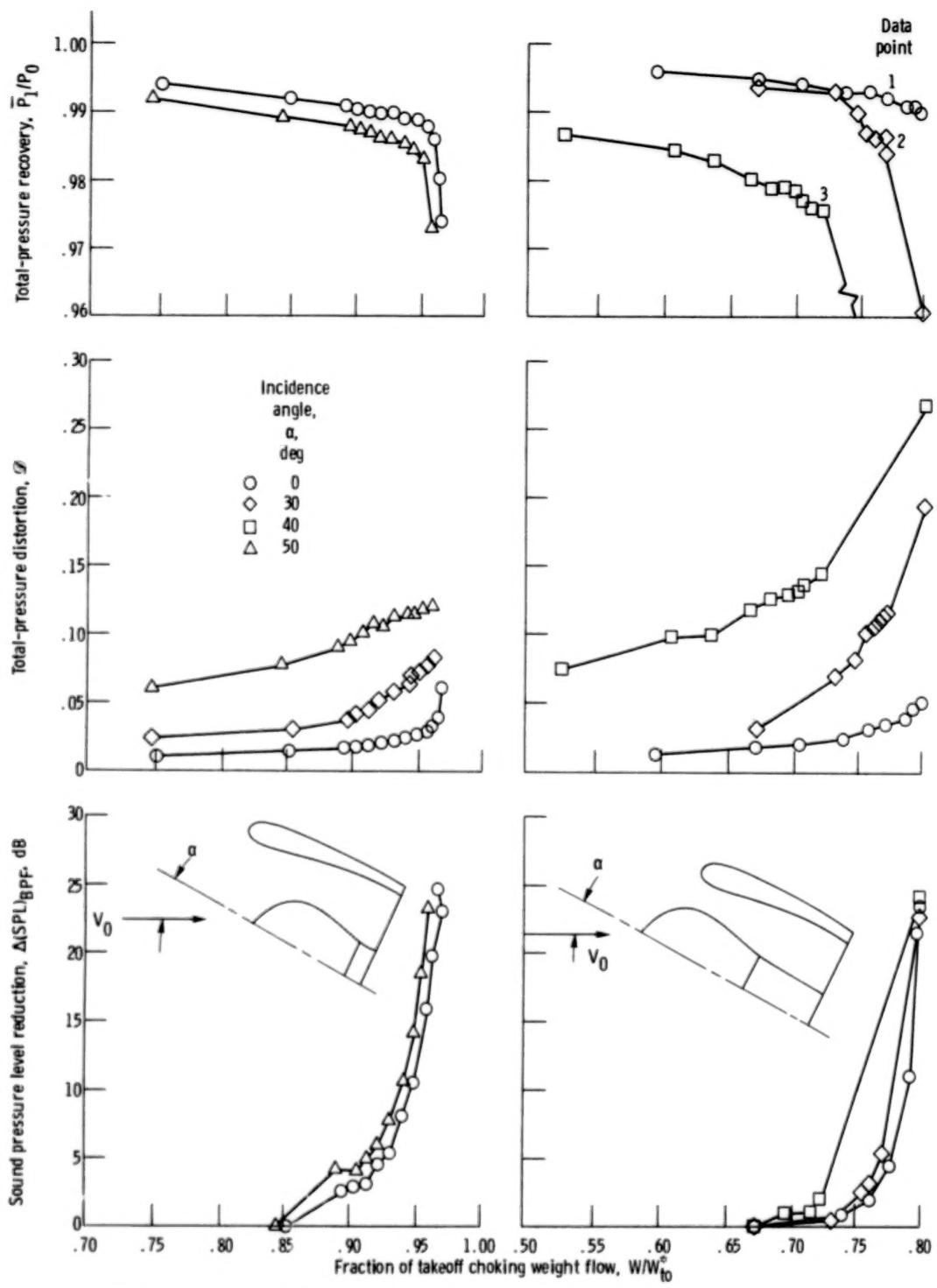
28.

Figure 11. - Effect of incidence angle on takeoff and approach aeroacoustic performance. Long diffuser; center-body A; free-stream velocity, V_0, 41 m/sec (80 knots).
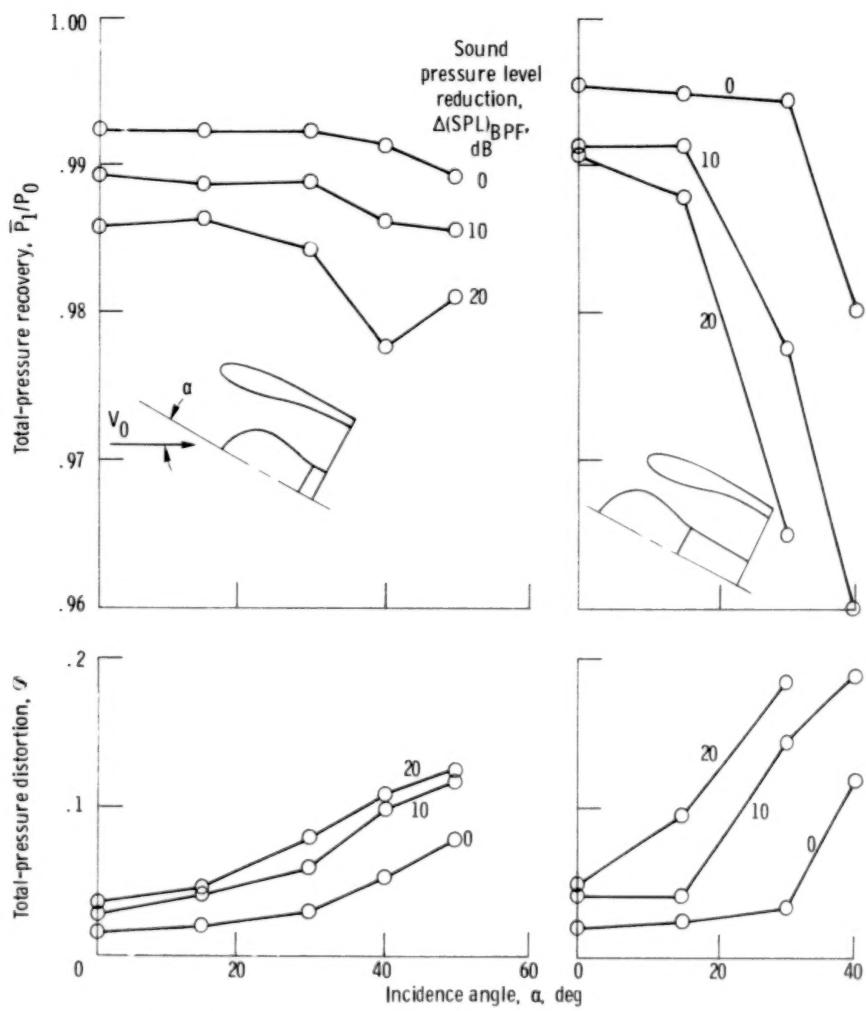
(a) Centerbody in takeoff position; test model 1.

(b) Centerbody in approach position; test model 5.

29

(a) Centerbody in takeoff position; test model 1.

(b) Centerbody in approach position; test model 5.

Figure 12. - Comparison of takeoff and approach aeroacoustic performance at a free-stream velocity V_0 of 41 m/sec (80 knots). (Data obtained from a crossplot of fig. 11.)
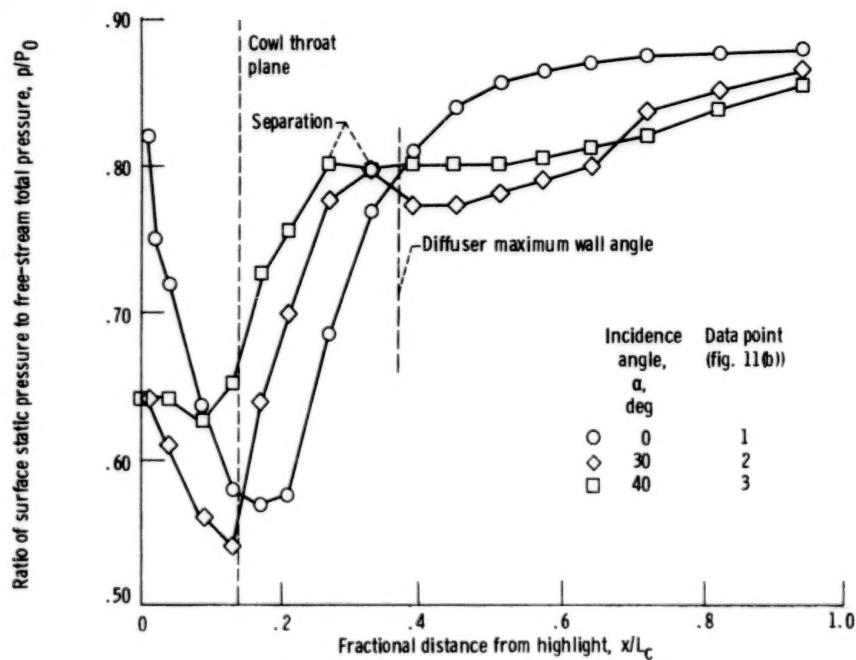
(a) Inlet cowl axial static-pressure distribution on windward side.
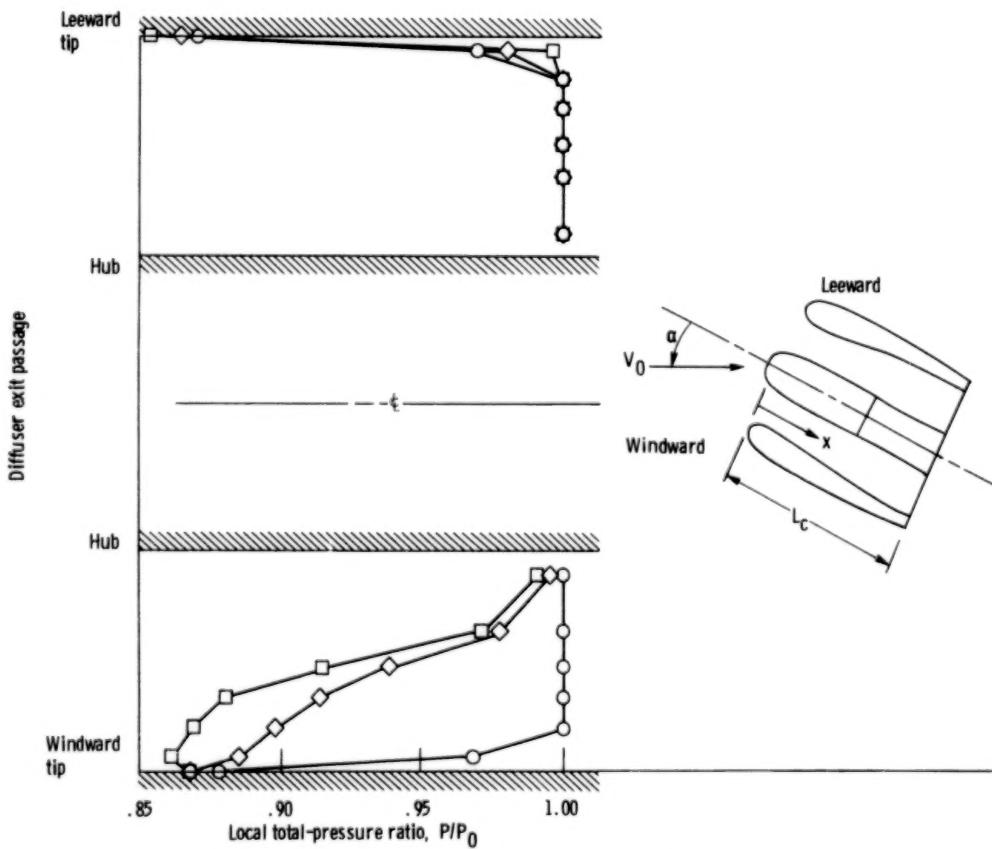
(b) Diffuser exit radial total-pressure distribution.

Figure 13. - Inlet static- and total-pressure distributions measured with test model 5 (approach configuration), indicating local flow separation within diffuser. Freestream velocity, V_0, 41 m/sec (80 knots).

31
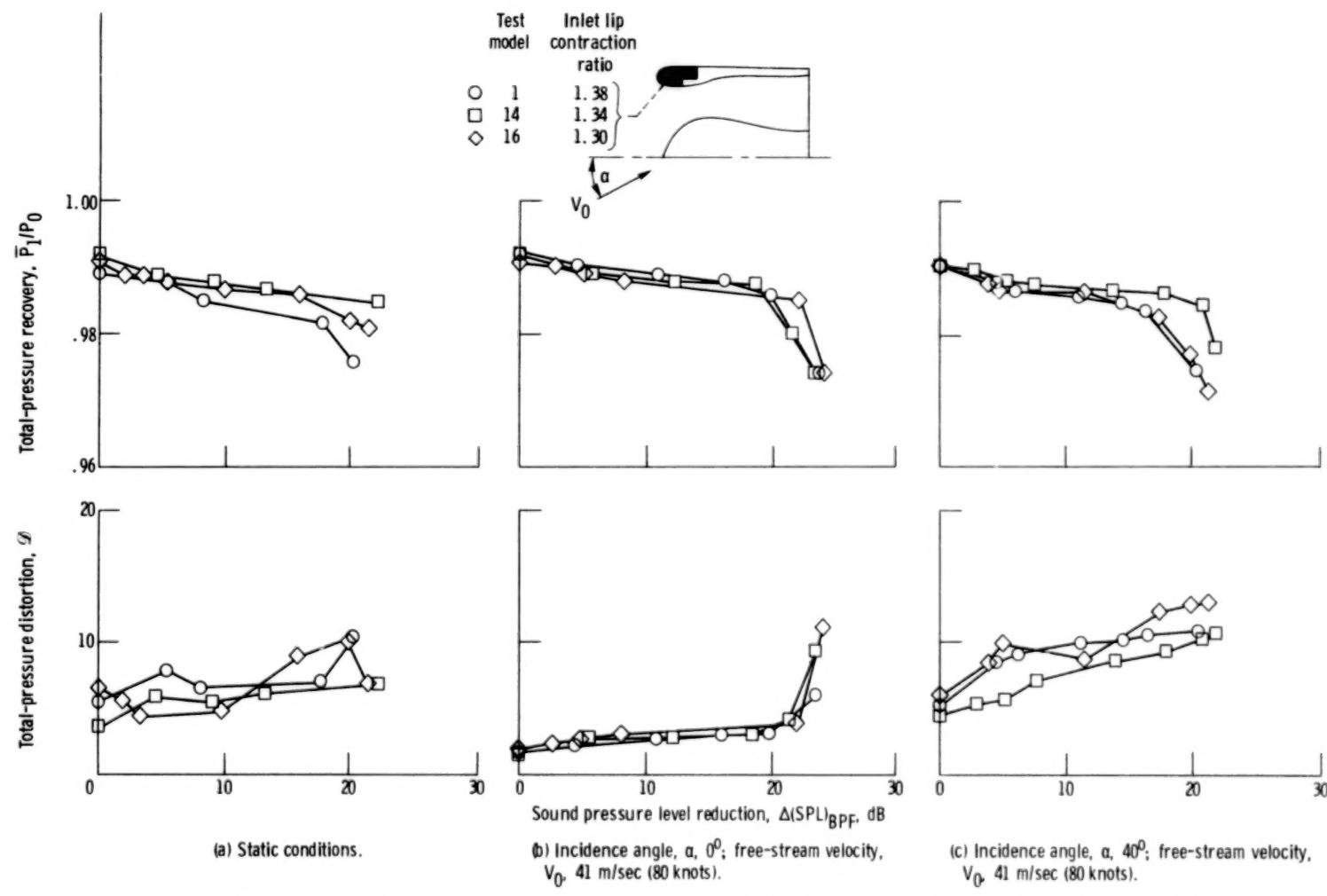
Figure 14. - Effect of inlet lip contraction ratio on aeroacoustic performance with centerbody in takeoff position. Long diffuser; centerbody A.
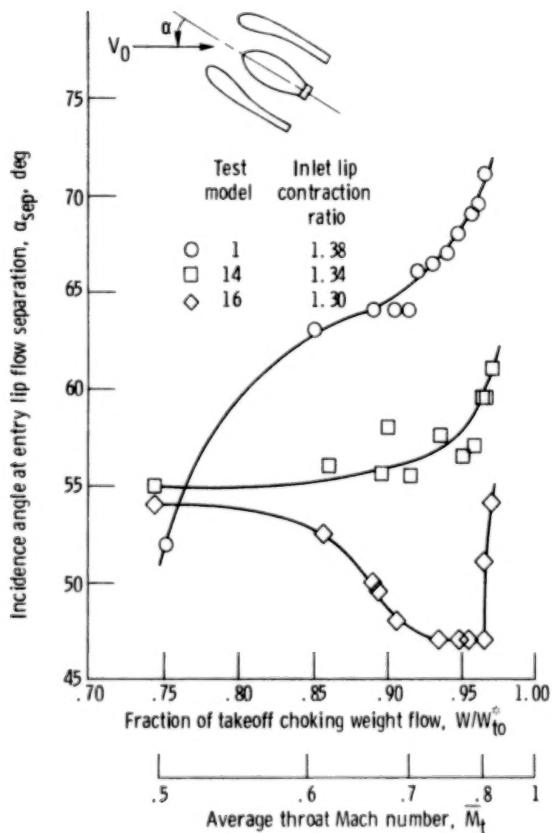
Figure 15. – Effect of inlet lip contraction ratio on incidence angle producing inlet flow separation. Inlet in takeoff configuration with centerbody retracted. Free-stream velocity, V_0, 41 m/sec (80 knots).

33.
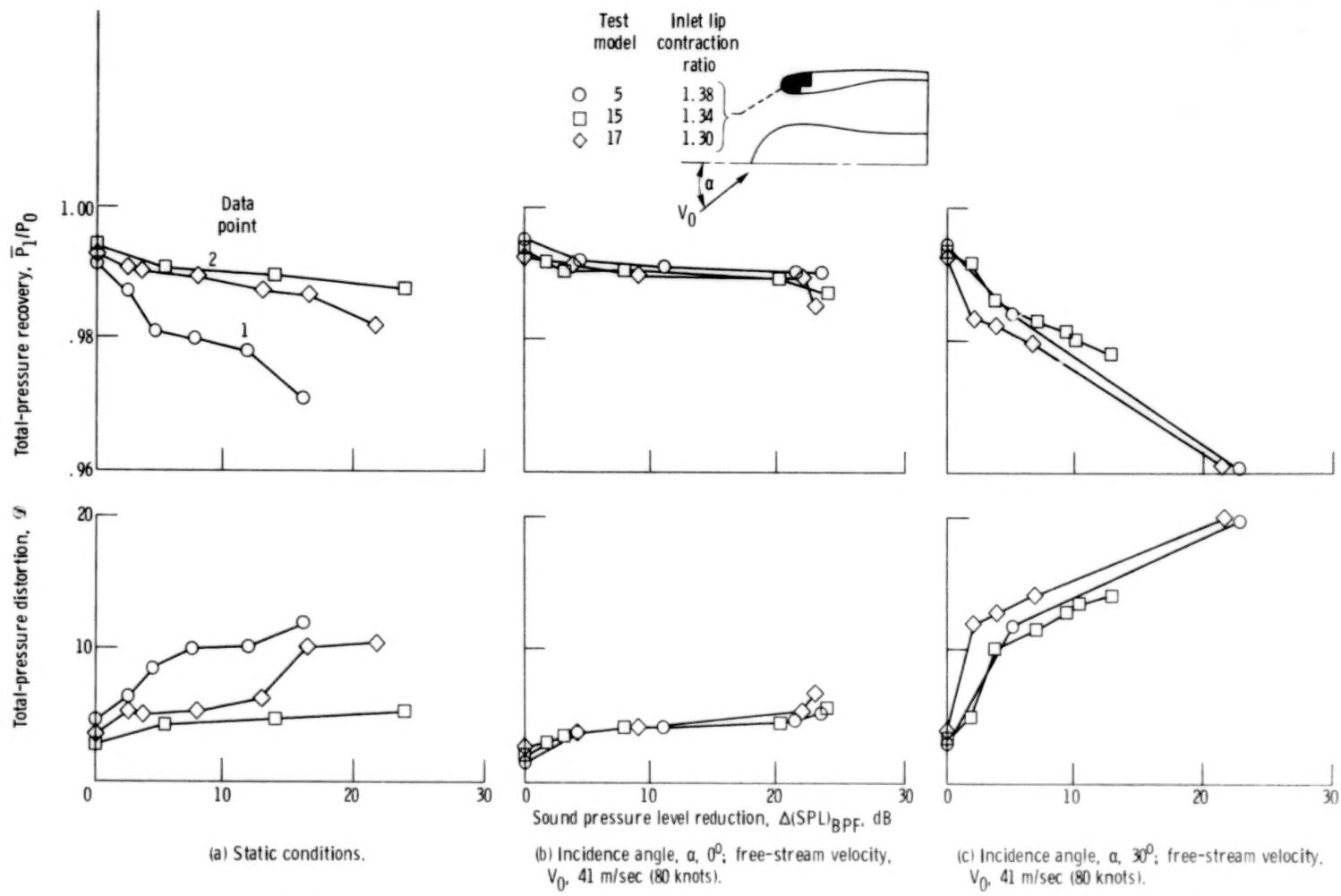
Figure 16. - Effect of inlet lip contraction ratio on aeroacoustic performance with centerbody in approach position. Long diffuser; centerbody A.
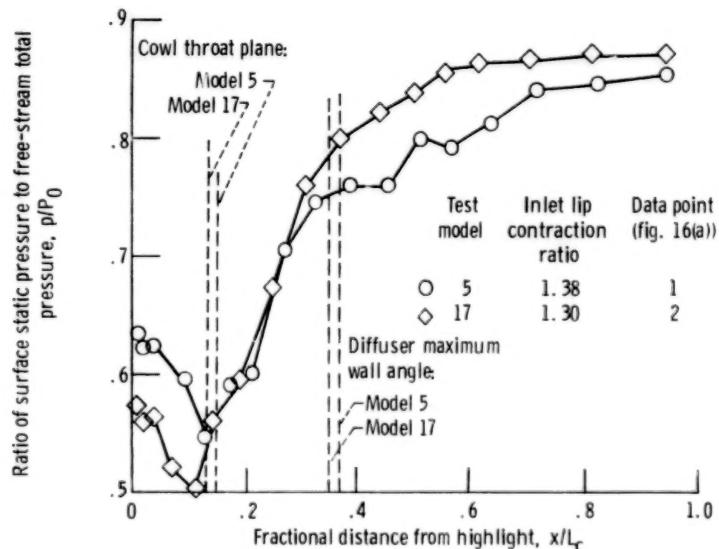
34.

(a) Inlet cowl axial static-pressure distribution.
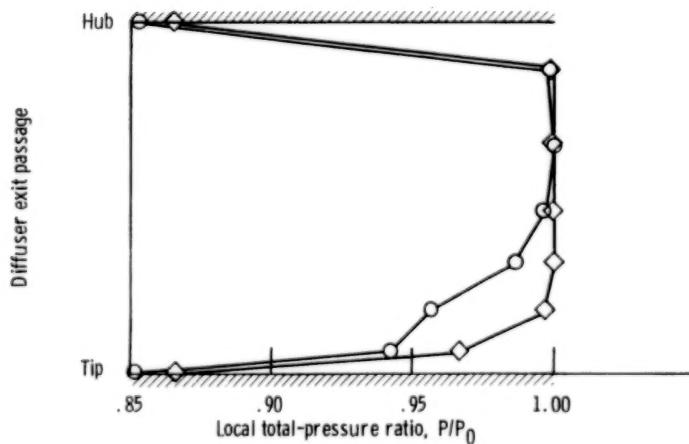
(b) Diffuser exit radial total-pressure distribution.

Figure 17. - Inlet static- and total-pressure distributions measured
with test models 5 and 17, indicating presence of local diffuser
separation for model 5. Data obtained at static conditions. Air-
flow ratio, W/W^*, 0.976.

35.
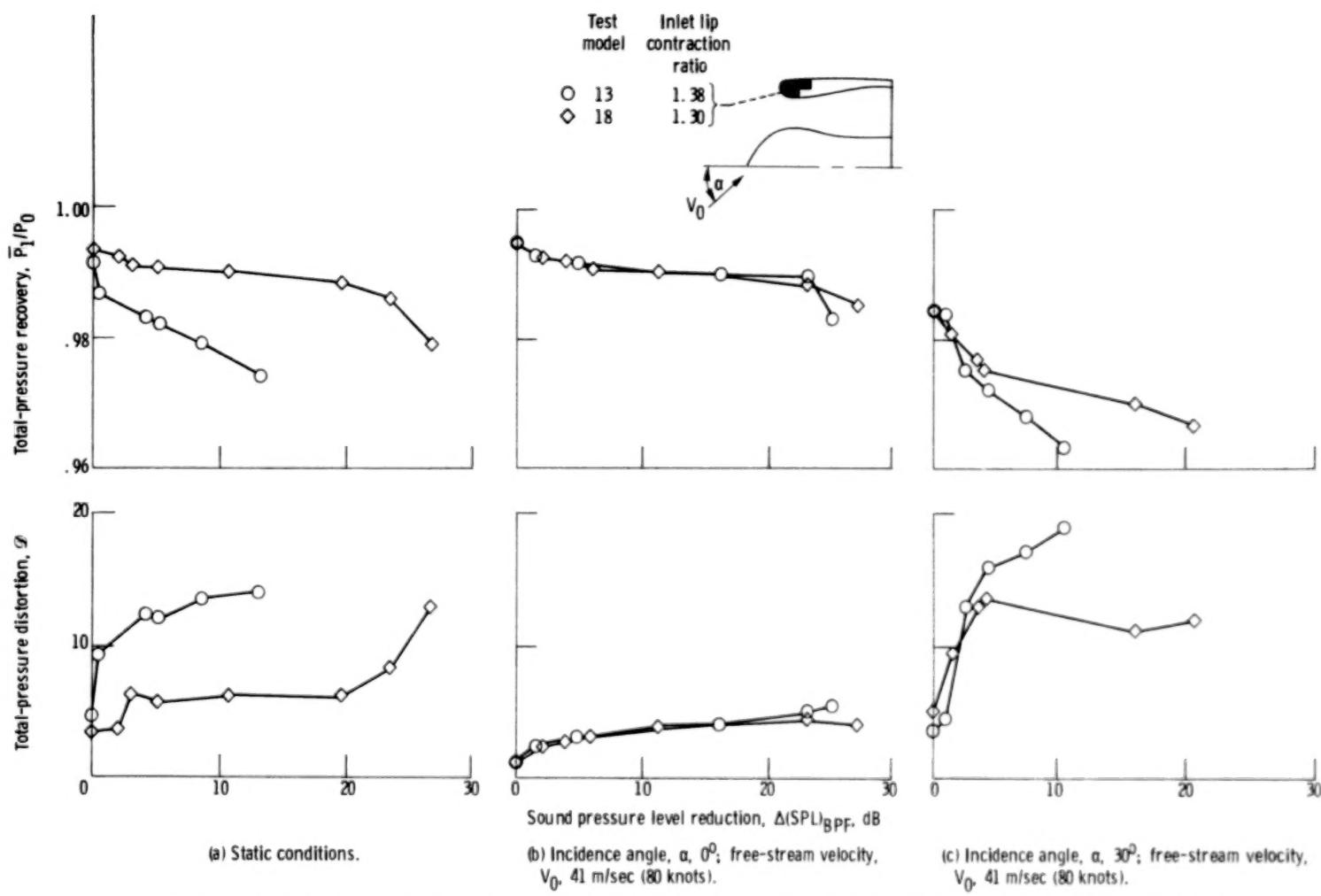
Figure 18. - Effect of inlet lip contraction ratio on aeroacoustic performance with centerbody in approach position. Short diffuser; centerbody F.
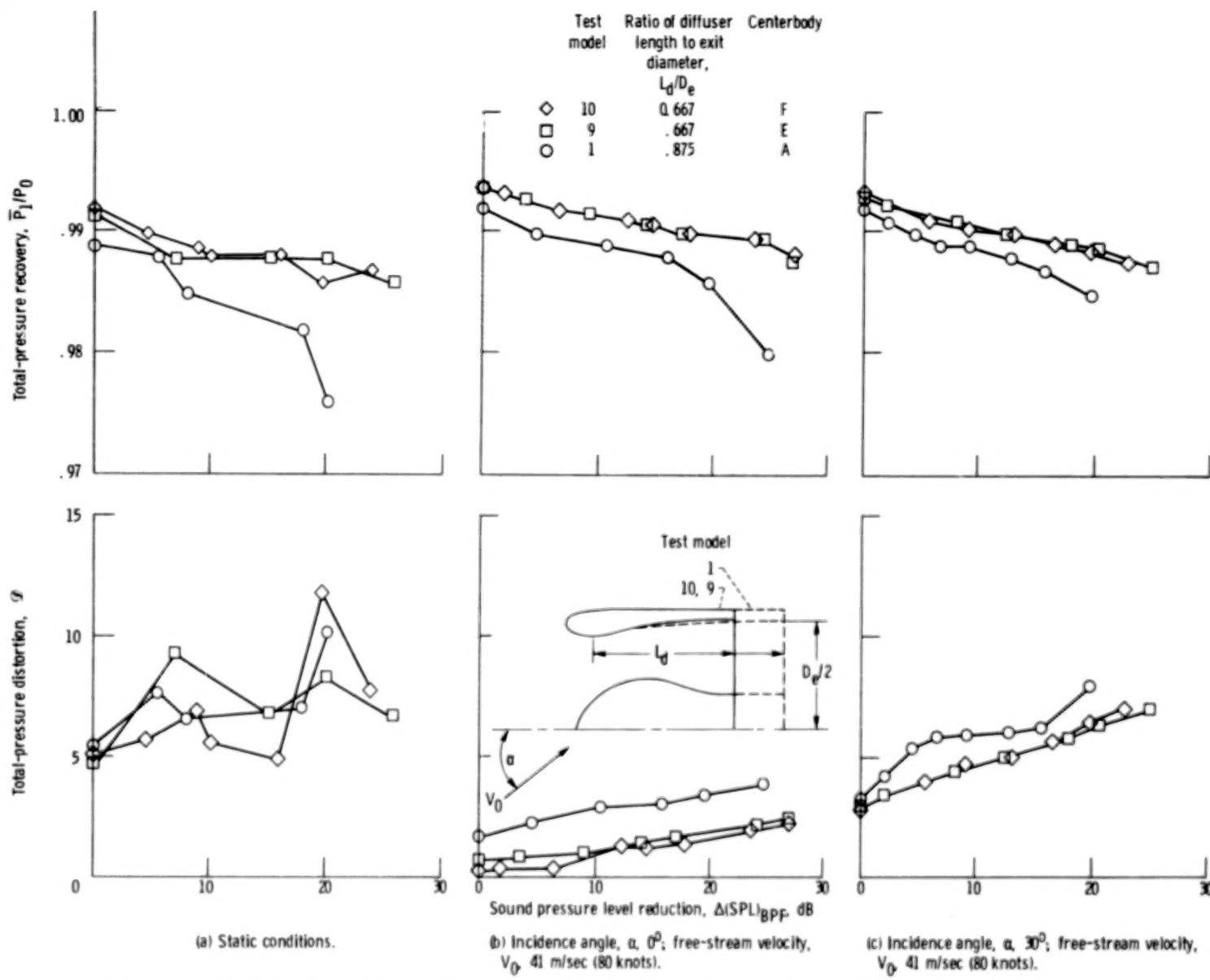
Figure 19. - Effect of diffuser length on inlet aeroacoustic performance with centerbody in takeoff position. Inlet lip contraction ratio, 1.38; diffuser area ratio, A_e/A_t, 1.19.

(a) Static conditions.

(b) Incidence angle, α, $0°$; free-stream velocity, V_0, 41 m/sec (80 knots).

(c) Incidence angle, α, $30°$; free-stream velocity, V_0, 41 m/sec (80 knots).

37.
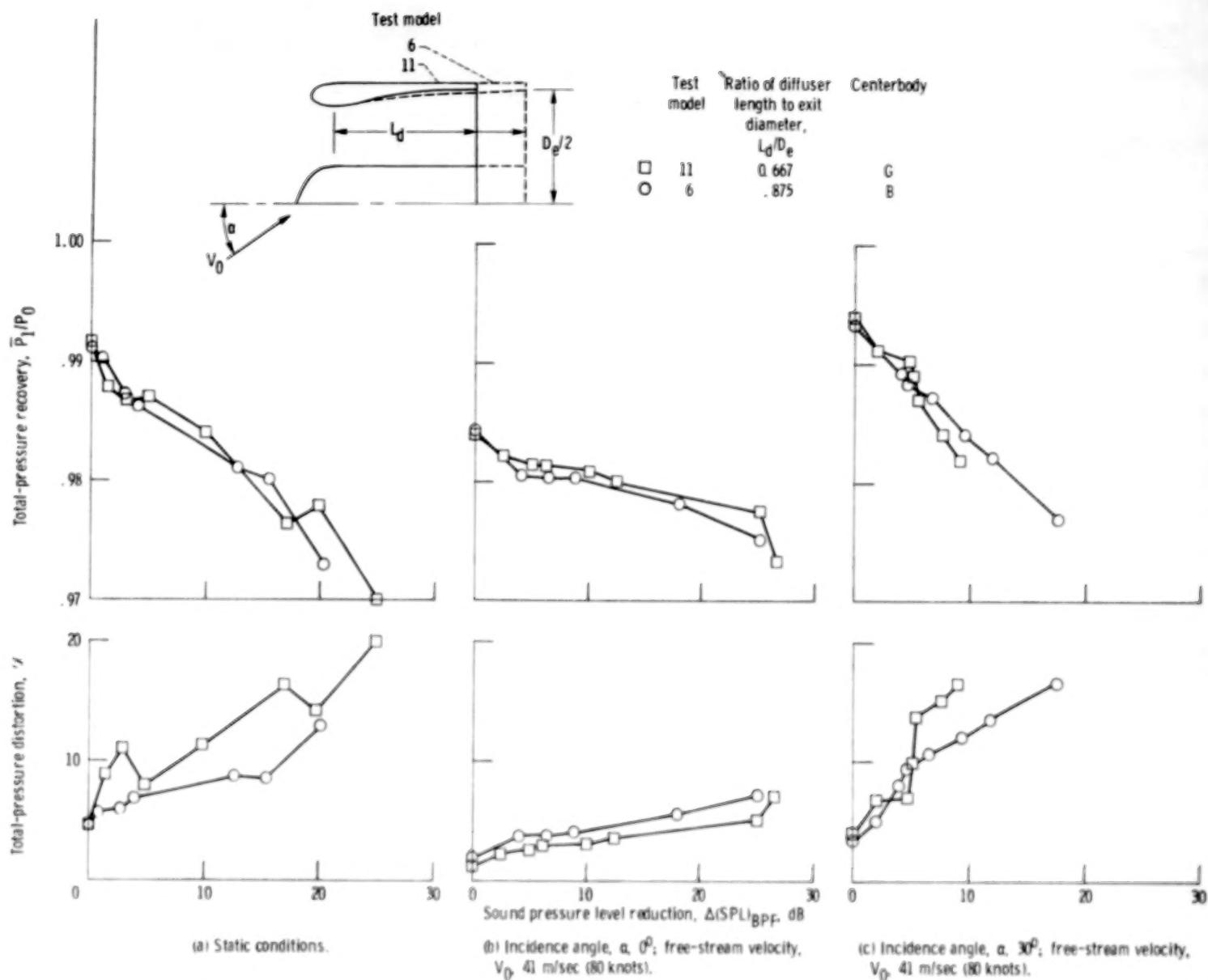
Figure 20. - Effect of diffuser length on inlet aeroacoustic performance with centerbody in approach position. Inlet lip contraction ratio, 1.38; diffuser area ratio, A_e/A_t, 1.38.

38.
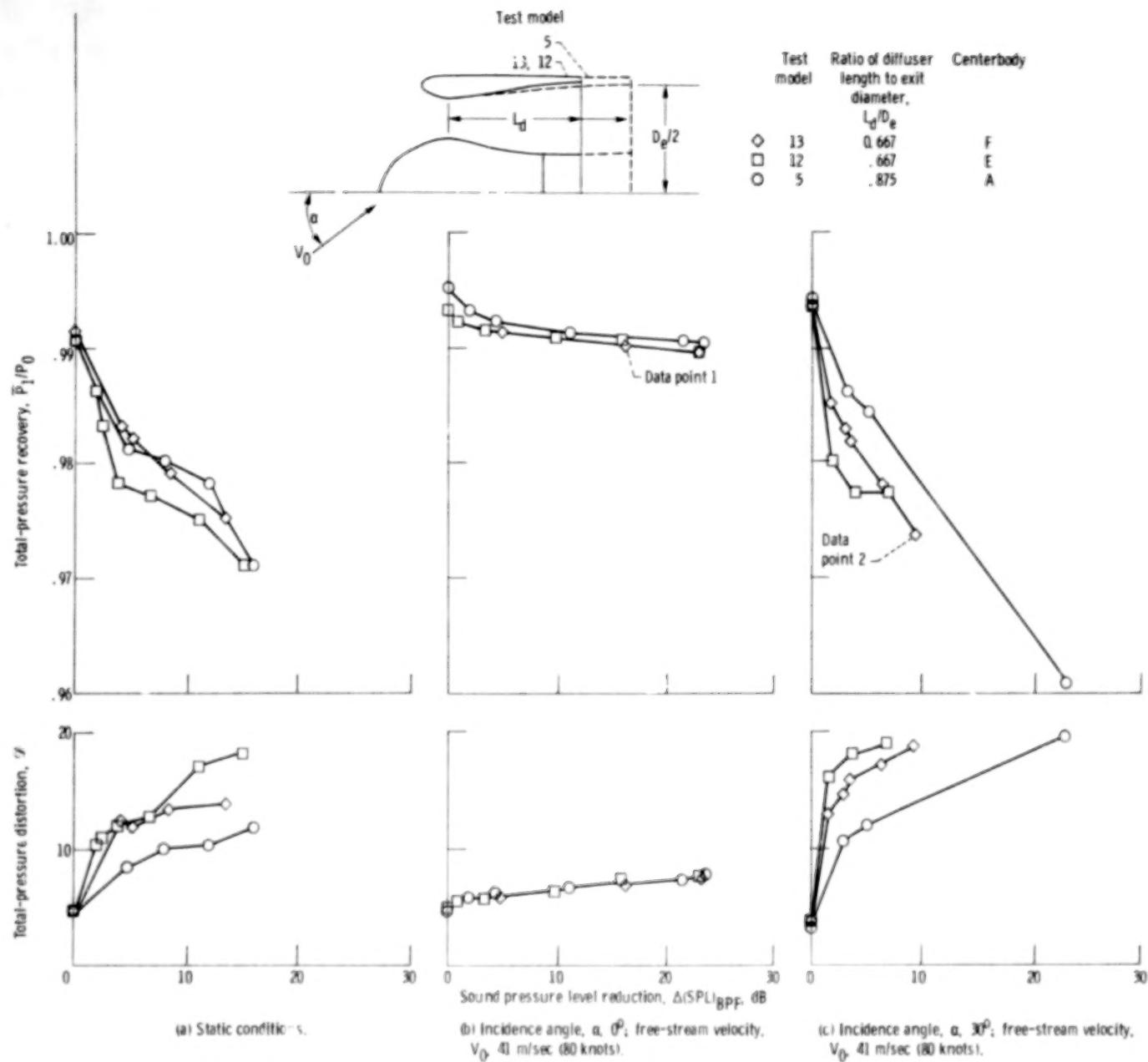
Figure 21. - Effect of diffuser length on inlet aeroacoustic performance with centerbody in approach position. Inlet lip contraction ratio, 1.38; diffuser area ratio, A_e/A_t, 1.49.
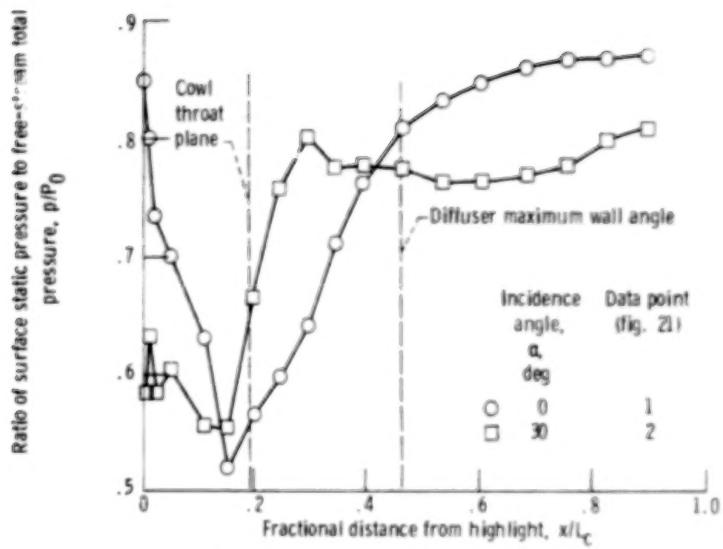
(a) Inlet cowl axial static-pressure distribution on windward side.
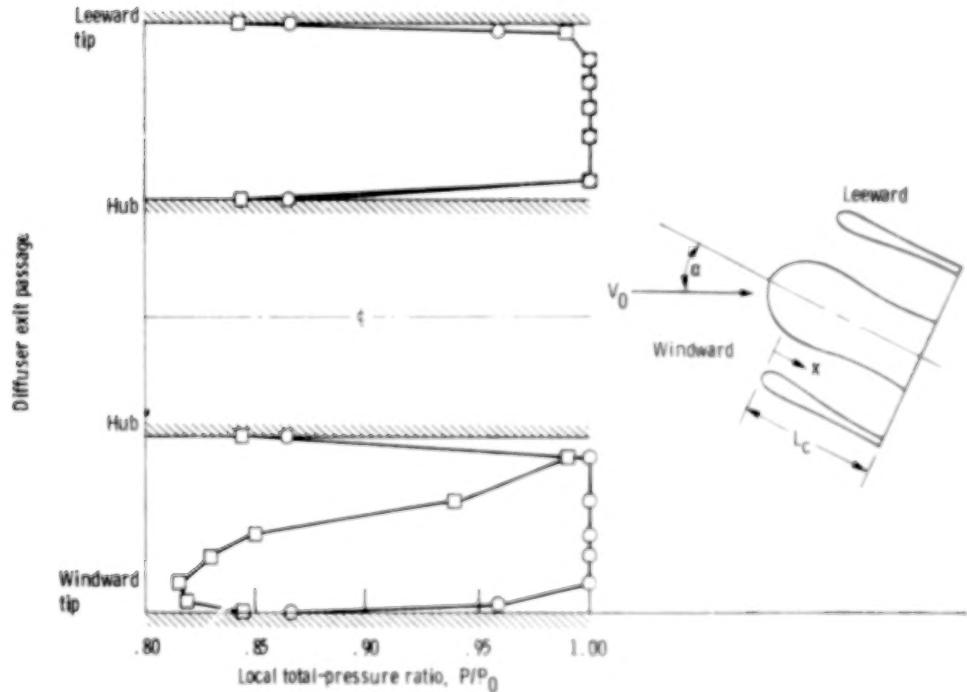
(b) Diffuser exit radial total-pressure distribution.

Figure 22. - Inlet static- and total-pressure distributions measured with model 13 (approach configuration), indicating diffuser flow separation at 30° incidence angle. Free-stream velocity, V_0, 41 m/sec (80 knots)
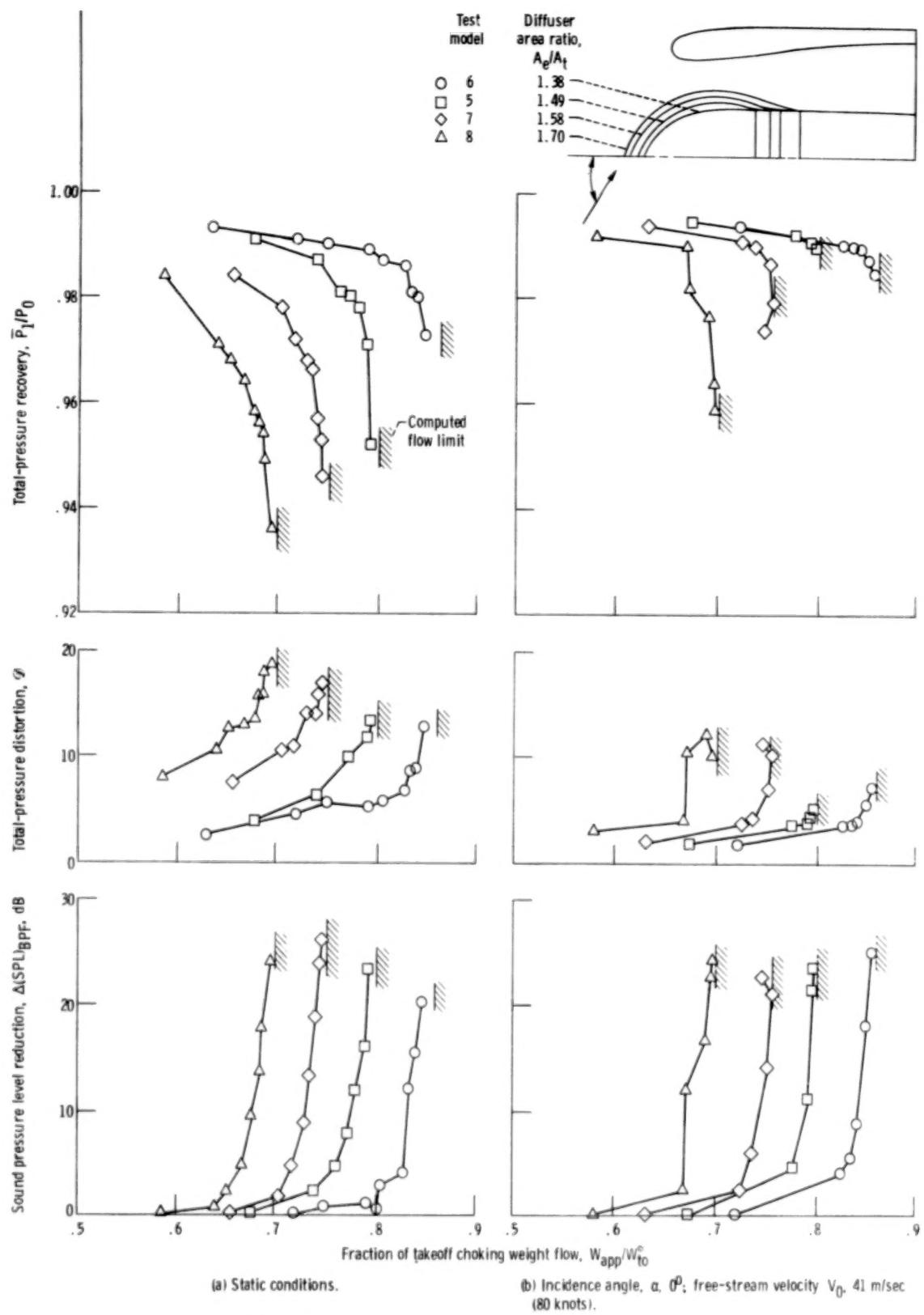
Figure 23. – Effect of diffuser area ratio at approach on variation of inlet aeroacoustic performance with weight flow.

(a) Static conditions.

(b) Incidence angle, α, 0^0; free-stream velocity V_0, 41 m/sec (80 knots).

41

(c) Incidence angle, α, 30°; free-stream velocity, V_0, 41 m/sec (80 knots).
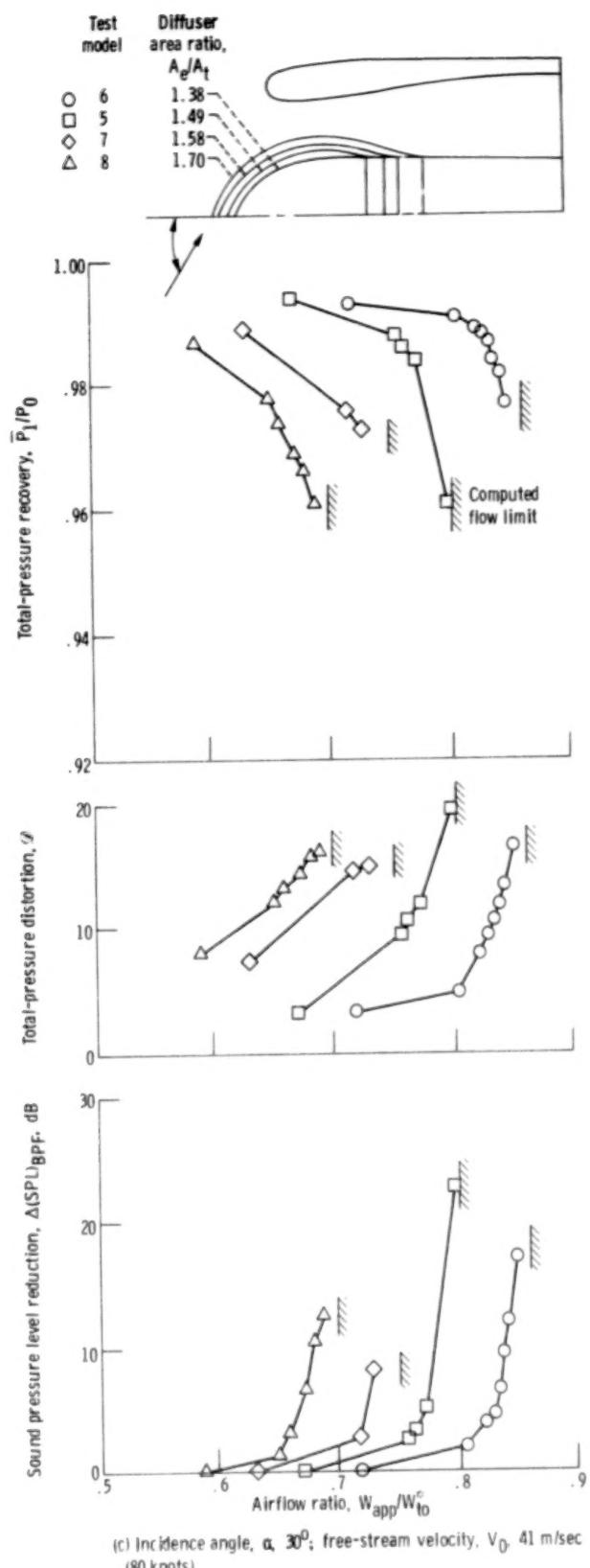
Figure 23. - Concluded.
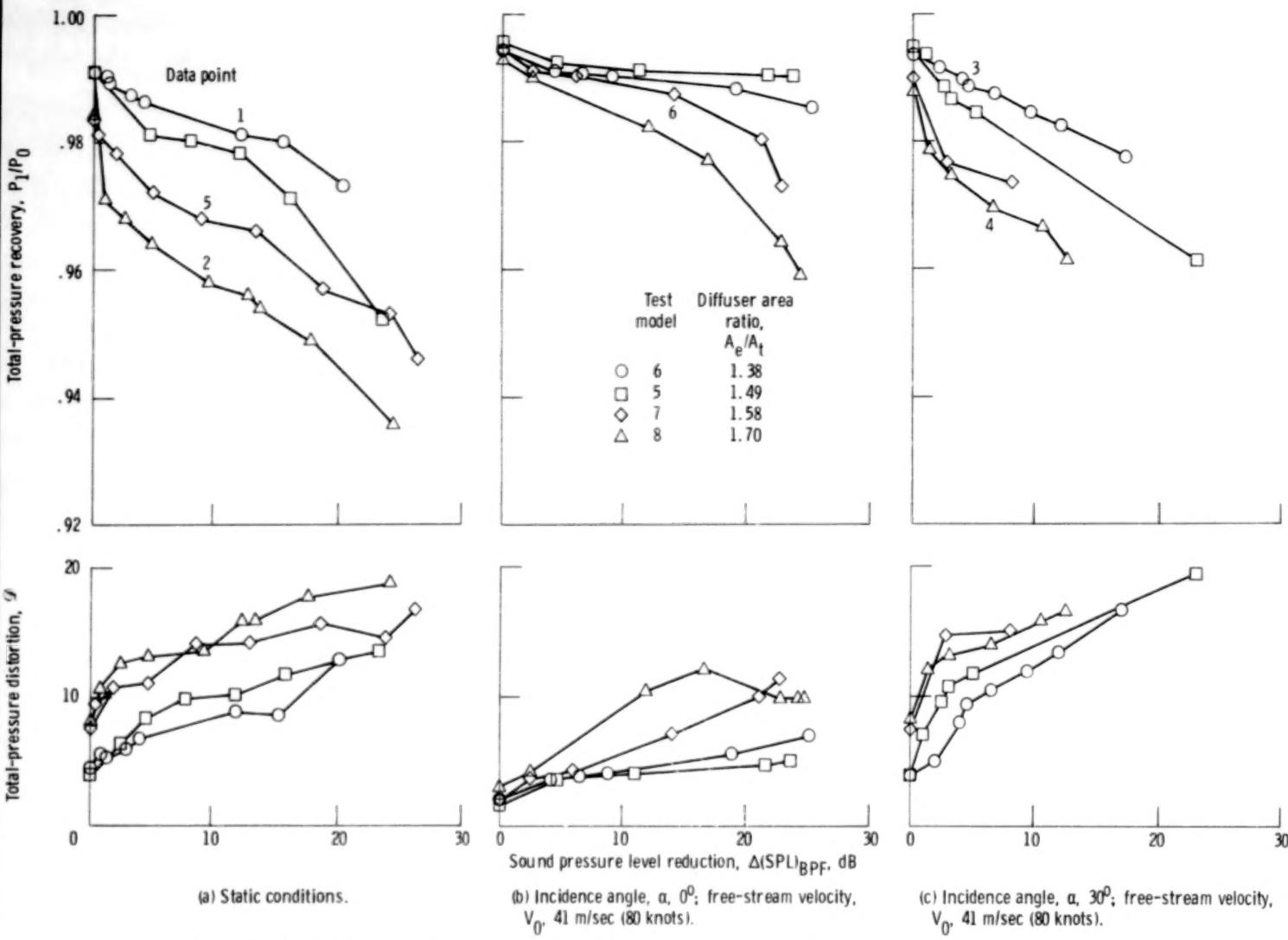
Figure 24. - Effect of diffuser area ratio at approach on variation of inlet aerodynamic performance with sound pressure level reduction.

43.

(a-1) Inlet cowl axial static-pressure distribution.
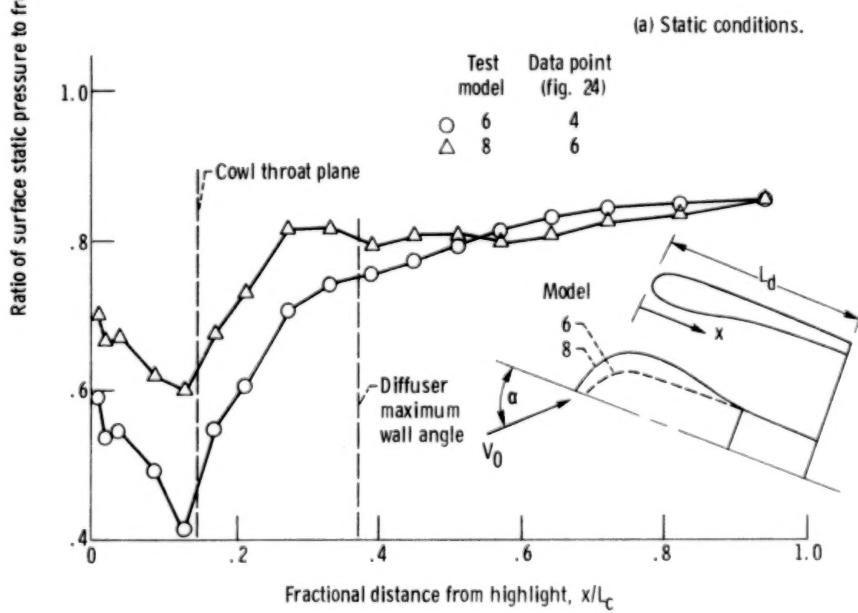
(a) Static conditions.

(a-2) Diffuser exit radial total-pressure distribution.

(b-1) Inlet cowl axial static-pressure distribution on windward side.

(b-2) Diffuser exit radial total-pressure distribution.

(b) Incidence angle, α, 30^0; free-stream velocity, V_0, 41 m/sec (80 knots).

Figure 25. - Comparison of static- and total-pressure distributions between smallest (test model 6) and largest (test model 8) area ratio diffusers at approach.

44.
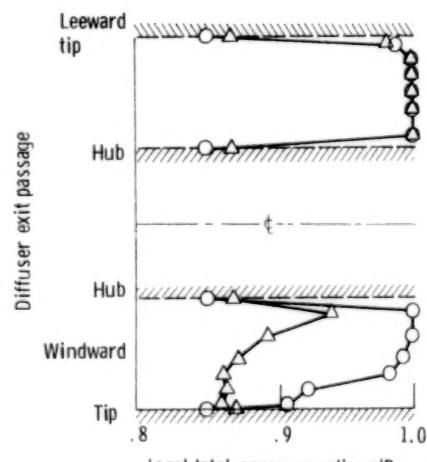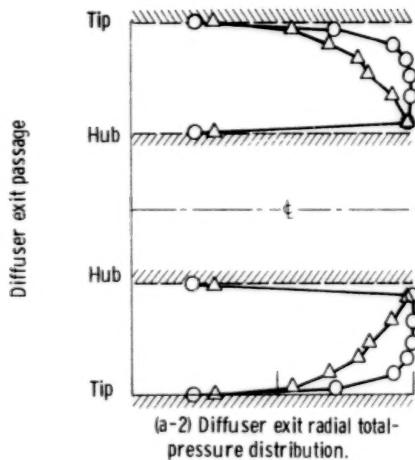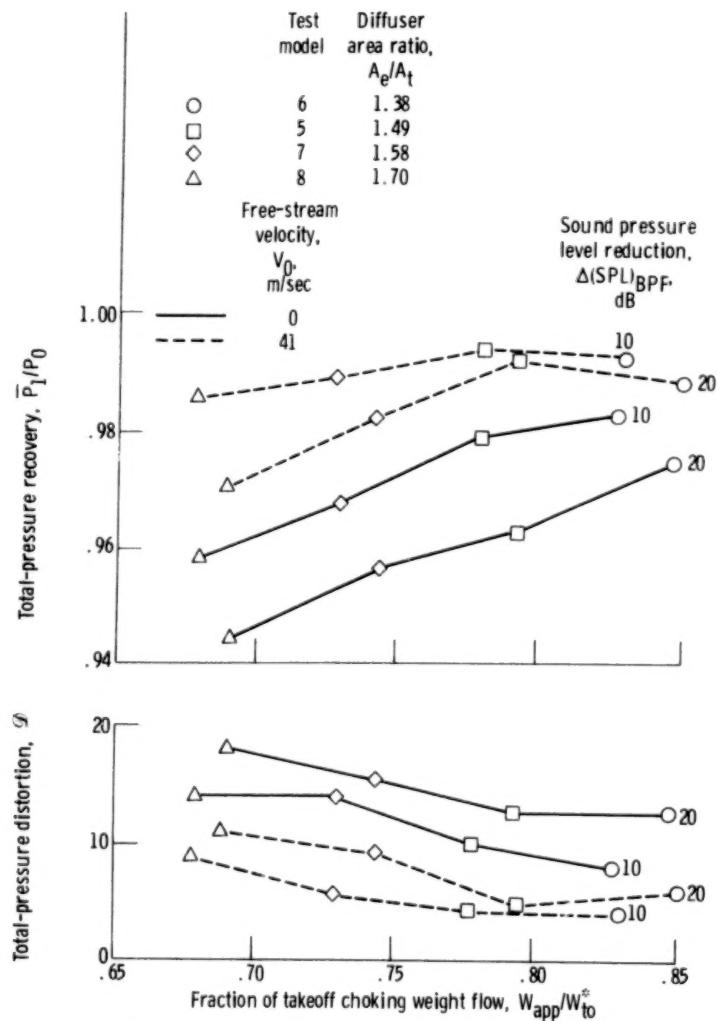
Figure 26. – Improvement in aeroacoustic performance at approach configuration due to free-stream velocity. Incidence angle, α, 0°.
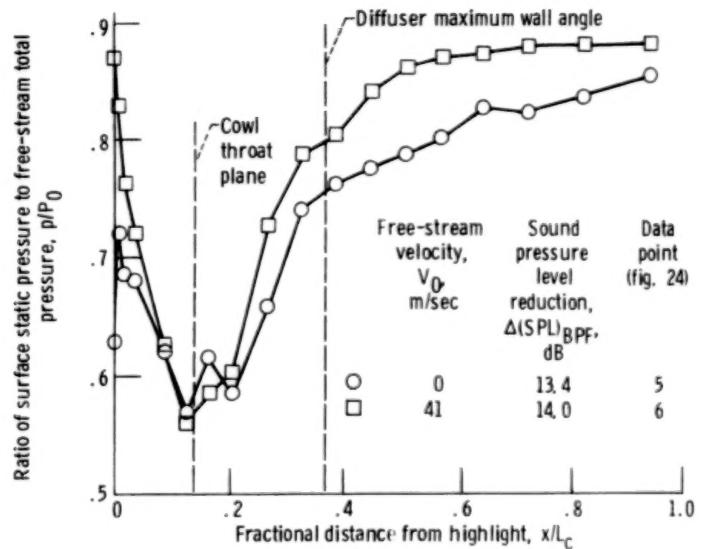
(a) Inlet cowl axial static-pressure distribution.
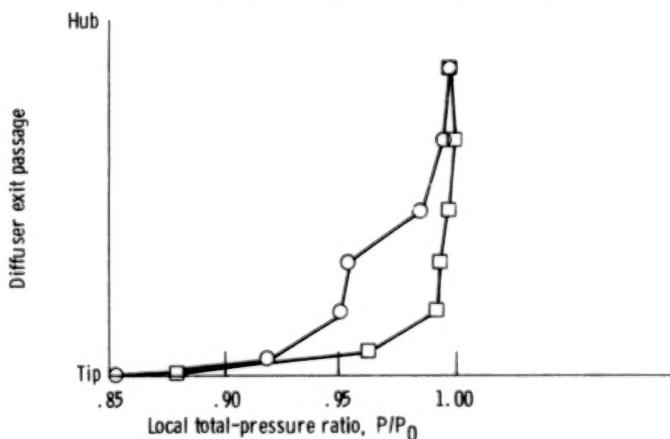
(b) Diffuser exit radial total-pressure distribution.

Figure 27. - Effect of forward velocity on test model 7 static- and total-pressure distributions. Diffuser area ratio, A_e/A_t, 1.58.

1. Report No. NASA TP-1132	2. Government Accession No.	3. Recipient's Catalog No.
4. Title and Subtitle EFFECT OF DESIGN CHANGES ON AERODYNAMIC AND ACOUSTIC PERFORMANCE OF TRANSLATING-CENTERBODY SONIC INLETS		5. Report Date February 1978
		6. Performing Organization Code
7. Author(s) Brent A. Miller		8. Performing Organization Report No. E-9283
		10. Work Unit No. 505-03
9. Performing Organization Name and Address National Aeronautics and Space Administration Lewis Research Center Cleveland, Ohio 44135		11. Contract or Grant No.
		13. Type of Report and Period Covered Technical Paper
12. Sponsoring Agency Name and Address National Aeronautics and Space Administration Washington, D.C. 20546		14. Sponsoring Agency Code

15. Supplementary Notes

16. Abstract

An experimental investigation was conducted to determine the effect of design changes on the aerodynamic and acoustic performance of translating-centerbody sonic inlets. Scale-model inlets were tested in the Lewis Research Center's V/STOL wind tunnel. The effects of center-body position, entry lip contraction ratio, diffuser length, and diffuser area ratio on inlet total-pressure recovery, distortion, and noise suppression were investigated at static conditions and at forward velocity and angle of attack. With the centerbody in the takeoff position (retracted), good aerodynamic and acoustic performance was attained at static conditions and at forward velocity. At 0° incidence angle with a sound pressure level reduction of 20 dB, the total-pressure recovery was 0.986. Pressure recovery at 50° was 0.981. With the centerbody in the approach position (extended), diffuser flow separation occurred at an incidence angle of approximately 20°. However, good performance was attained at lower angles. With the centerbody in the takeoff position the ability of the inlet to tolerate high incidence angles was improved by increasing the lip contraction ratio. However, at static conditions with the centerbody in the approach position, an optimum lip contraction ratio appears to exist, with both thinner and thicker lips yielding reduced performan...

17. Key Words (Suggested by Author(s)) Inlet design; Sonic inlet; Choked inlet; Noise reduction; High Mach number inlet; Wind tunnel tests	18. Distribution Statement Unclassified - unlimited STAR Category 02		
19. Security Classif. (of this report) Unclassified	20. Security Classif. (of this page) Unclassified	21. No. of Pages 47	22. Price* A03